JOURNAL OF GEOPHYSICAL RESEARCH, VOL. 101, NO. C9, PAGES 20,771–20,797, SEPTEMBER 15, 1996

Numerical simulation of the dynamics of sea spray over the waves

P.G. Mestayer

Laboratoire de Mécanique des Fluides, Unité de Recherche Associée au Centre National de la Recherche Scientifique Ecole Centrale de Nantes, Nantes, France

A.M.J. Van Eijk and G. De Leeuw

Physics and Electronics Laboratory, Netherlands Organization for Applied Scientific Research TNO, Den Haag, the Netherlands

B. Tranchant

Laboratoire de Mécanique des Fluides, Unité de Recherche Associée au Centre National de la Recherche Scientifique Ecole Centrale de Nantes, Nantes, France

Abstract. SeaCluse is a code describing and quantifying the nonlinear interactions between spray droplet concentrations and the scalar fields of water vapor concentration and temperature in the marine atmospheric surface layer as a function of the basic micrometeorological parameters. It is currently developed to simulate most of the dynamics of the evaporating sea spray droplets, their transformations, and their influence on the structure of the marine lower atmosphere. It includes two parts, a "preprocessor" computing the air flow structure and droplet trajectories over the waves in the absence of turbulence and evaporation, and a "main program" computing along the vertical the horizontally averaged budgets of droplet and water vapor concentrations, and sensible heat, including the dynamic and thermodynamic air-droplet interactions. This paper presents the first simulations, without evaporation, which reveal several characteristic features of the spray droplet dynamics over the waves. The mean air flow induced by the wave motion generates an efficient transport of many droplets up to the wave crest level or slightly higher, where they accumulate. In contrast, turbulence appears to be a rather inefficient process to elevate further the droplets that have nonnegligible weight and inertia (and an efficient process for very small droplets). The residence times in the air T_{fly} of droplets larger than 90 μm in radius do not increase much, compared to their values in still air or over a flat surface, and they increase with increasing wind speed much less rapidly than the wave height H_s: $T_{fly} \sim U^{0.3}$ while $H_s \sim U^2$. Above the wave crest, the droplet concentrations are several orders of magnitude smaller than between wave troughs and crests. The precision of the turbulent diffusivity model for droplets therefore appears crucial to correctly infer the spray surface source function from concentration measurements in the atmosphere.

1. Sea Spray Modelling

1.1 Sea Spray in the Atmosphere

Aerosols play an important role in the marine atmospheric boundary layer, in meteorological processes, climatology, environmental processes, as well as in the field of propagation of electrooptical radiation. Suspended aerosols, by scattering and absorption of radiation, contribute to the attenuation of radiation in the electromagnetic transmission windows. This reduces the performance of electrooptical systems and limits electrooptical surveillance of the marine boundary layer and the sea surface from aircraft and satellites. The reduced albedo may also be of importance for climatology, as evidenced by recent studies of global warming negative feedback effects.

On a micrometeorological scale, aerosols contribute to the moisture and heat budgets near the sea surface [*Wu*, 1974; *Ling and Kao*, 1976; *Andreas*, 1992]. Since the ocean acts both as a source and a sink for atmospheric aerosols, the aerosol droplets may transfer water vapor, heat, pollutants, and bacteria through the air-sea interface. At higher levels, sea-salt particles shrink by evaporation or grow by condensation through interaction with the humidity field. Hence they play a role in the transport of matter, heat, and water vapor throughout the marine boundary layer and are important to larger scale meteorological processes and climatology. In addition, small droplets may act as condensation nuclei and are therefore important in the formation of fog and clouds.

In view of the above, adequate descriptions of the particle size distributions for the ambient atmospheric conditions are required to explain a wide range of processes in the marine atmospheric boundary layer (MABL). The Navy Aerosol Model (NAM) [*Gathman*, 1983] is one of the most widely accepted and used models to assess the propagation characteristics of electrooptical radiation. NAM is included in the LOWTRAN code [*Kneizys et al.*, 1983]. It is an empirical model, based on an extensive data set composed of observations made at a variety of geographical locations. Over the years, NAM has been updated and improved with both experimental [*De Leeuw*, 1986] and theoretical [*Gerber*, 1985] evidence [*Hughes*, 1987; *Gathman*, 1989].

NAM applies to a single height of about 10 m above mean sea level (AMSL). Therefore additional modeling is required to infer the vertical profiles of aerosol concentration. The Navy Oceanic Vertical Aerosol Model (NOVAM) has been developed to this

Paper number 96JC01425.
0148-0227/96/96JC-01425$09.00

end [*Gathman*, 1989; *De Leeuw et al.*, 1989]. In NOVAM, the concentration of aerosol at deck height is provided by NAM, and the vertical distribution of aerosols is subsequently calculated with physical equations.

NAM and NOVAM have been validated for open ocean regions. However, they do not apply below about 10 m AMSL. Yet, this region is important because an important part of the aerosol dynamics takes place in the surface layer, and the development of models for the marine atmospheric boundary layer requires a comprehensive description of the processes near the air-sea interface.

Aerosol behavior near the air-sea interface is difficult to describe because it results from a large number of coupled dynamic and physical processes. When wave breaking occurs, air is entrained into the water. The air breaks up into bubbles, which rise owing to their buoyancy. When they reach the surface and burst, film and jet droplets are produced. Film droplets result from the breaking of the thin water film covering the bubble where it protrudes upward through the water surface, and jet droplets result from the breaking up of the water jet that is subsequently formed [*Blanchard*, 1963; *MacIntyre*, 1972; *Blanchard and Woodcock*, 1980]. The production of film and jet droplets from both single bubbles and bubble plumes has been the subject of extensive experimental studies [e.g., *Blanchard*, 1963, 1983; *Monahan et al.*, 1982; *Mestayer and Lefauconnier*, 1988; *Spiel*, 1992]. An analytical description of the jet droplet production has recently been provided by *Dekker and De Leeuw* [1993], based on the analyses of *MacIntyre* [1968, 1972]. In addition to the film and jet droplets, spume droplets are produced by tearing from the wave crest, when the wind speed exceeds about 9 m/s [*Monahan et al.*, 1986; *Wu*, 1990; *Andreas*, 1992].

The freshly produced droplets are transported upward by turbulent diffusion and convective flow, which are counterbalanced by gravitational forces. While they are airborne, they interact with the scalar fields of temperature and humidity by exchanges of heat and moisture.

1.2 Vertical Flux of Spray

The number and size distribution of sea spray aerosols that are produced by breaking waves are described by the surface source function, often expressed as $\partial F/\partial r$, the number of droplets of radius r produced at the sea surface per m^2, per second, per μm increment in r, where r is droplet initial radius. This function is sometimes replaced by $\partial F/\partial r_{80}$, where r_{80} is droplet radius at 80% relative humidity. *Monahan et al.* [1982, 1986] presented a source function that consists of two modes, i.e., a bubble-mediated and a spume droplet source function. Alternative formulations have been given by *Fairall et al.* [1983] [see also *Miller and Fairall*, 1988], *De Leeuw* [1990a] and *Andreas* [1990b, 1992]. However, there is no report of direct measurements of the upward surface flux of droplets at sea, and the extension of laboratory studies to oceanic conditions is not straightforward either [e.g., *Ling and Kao*, 1976; *Mestayer and Lefauconnier*, 1988].

Few measurements exist of the concentration of aerosols below ship deck level (see, e.g., *De Leeuw* [1989b, 1993] for an overview). Until recently, the particle concentrations were assumed to increase exponentially toward the sea surface [*Blanchard and Woodcock*, 1980]. *De Leeuw* [1986, 1987] provided experimental evidence that the profiles are not always logarithmic, and hypothesized that the aerosols are temporarily trapped in rotor-like eddies generated by the wave motion, which results in longer suspension times. Alternatively, *Wu* [1990] suggested that the spume droplet production by the wave tearing mechanism was to be held responsible for the nonlogarithmic profiles.

It must be understood that the assessment of the surface source function is the key to understanding and modeling the spray behavior and influence, and vice versa. Since this function cannot be measured directly at present, two rationales have been used to infer it from measurements, "below-up" and "above-down". The below-up approach consists in tracing and modeling the behavior of whitecap bubbles from production to bursting, and in convoluting this model with empirical relationships between whitecap coverage and meteorological variables on the one hand, and with the spray production per bubble on the other hand. The works of *Monahan et al.* [1982, 1986], *Baldy* [1988], *Blanchard* [1963, 1983, 1989], *Dekker and De Leeuw* [1993], and *Spiel* [1992, 1994] address the successive stages of the process. This below-up approach could be qualified "direct", since it relates the surface flux of spray to its causes. In principle, the extension of the approach to the flux of spume droplets should be easy, since the number of stages is much reduced. But in practice, this extension has not been done yet, owing to the lack of reliable field data and because the laboratory simulations of spume droplet tearing are disputable (see, e.g., *Mestayer and Lefauconnier*'s [1988] discussion).

The above-down approach is "indirect" since it deduces the surface source function from its consequences, the aerosol concentrations in the air, usually measured well above sea level [*Fairall et al.*, 1983; *Fairall*, 1990; *Fairall et al.*, 1994; *Miller and Fairall*, 1988; *Wu*, 1979, 1989, 1990; *Wu et al.* 1984; *Smith et al.*, 1993]. Up to now, this approach used simple relationships between elevated concentrations and surface fluxes, based on the usual assumptions of the constant flux atmospheric surface layer over a flat surface, not taking into account the influence of the air flow over the waves on the droplet dynamics, the physicothermodynamic exchanges between air and spray, and their nonlinear coupling. Actually, this approach results in "effective" source functions that depend on the model assumptions that are used to derive them, and have validity only within the framework of this model. *Andreas* [1992] proposed an empirical synthesis of *Miller and Fairall*'s [1988] and *Wu et al.*'s [1984] results to infer a spectral shape on the whole range of droplet radii of interest. *Fairall et al.* [1994] combine this with *Monahan et al.*'s [1986] observations of whitecap coverage to infer the droplet spectrum dependence on wind speed. Yet, owing to the indirect ways used to derive this surface source function, there is still not consensus, and it is the object of a passionate debate [*Katsaros and De Leeuw*, 1994; *Andreas*, 1994].

1.3 Framework for Describing the Atmospheric Surface Layer with Spray

The above discussion shows that there is need for models giving a physical description of the behavior of marine spray droplets in the atmospheric surface layer close to the waves, that provide an operational framework for the analysis of the sparse experimental observations.

The theoretical framework for the analysis of measurements in the marine atmospheric surface layer is the constant flux layer assumption, the basis of Monin-Obukhov similarity theory. In the absence of strong convection, in the lower part of the atmospheric boundary layer over a flat surface the flow is horizontal on average and horizontally homogeneous. The surface layer is a few tens of meters thick. It is defined as the layer where the ref-

erence values of air density ρ_o, temperature T_o, and pressure p_o in Boussinesq approximations, have negligible variations with height and where the effect of Coriolis effect is also negligible [*Monin and Yaglom*, 1987]. The averaged budget equation of any transportable quantity ψ then reduces to

$$\frac{d\overline{\psi}}{dt} = \frac{\partial\overline{\psi}}{\partial t} + \overline{w\frac{\partial\psi}{\partial z}} = D_\psi \frac{\partial^2\overline{\psi}}{\partial z^2} + S_\psi \qquad (1)$$

where the coordinate system x, y, z is such that the x direction is horizontal and parallel to the mean wind and z is vertical upward, the wind vector components are u, v, w, respectively, the overbar indicates an ensemble average, d/dt is the particulate derivative, and D_ψ is the molecular diffusivity of ψ in air, or the molecular viscosity μ if ψ is momentum. Reynolds averaging is used to separate mean and fluctuating quantities:

$$\psi = \Psi + \psi' \;;\; \Psi = \overline{\psi} \;;\; \overline{\psi'} = 0 \qquad (2)$$

Usually the conditions are ergodic and stationary and the vertical component of the mean velocity $W = 0$. For momentum ρU and any inert gas concentration passively following the air flow, the additional term $S_\psi = 0$; *Fairall et al.* [1994] verified that the droplet relative contribution to the air momentum is at most $8\times10^{-6}\,U^{2.4}$, i.e., $< 10^{-1}$ when $U < 50$ m s^{-1} and $< 10^{-2}$ when $U < 20$ m s^{-1}. Using the continuity equation for an incompressible fluid, equation (1) then reduces to

$$\frac{\partial\Psi}{\partial t} = 0 = -\frac{\partial\overline{w'\psi'}}{\partial z} + D_\psi\frac{\partial^2\Psi}{\partial z^2} = -\frac{\partial}{\partial z}\left(\overline{w'\psi'} - D_\psi\frac{\partial\Psi}{\partial z}\right) \qquad (3)$$

$$\rho\frac{\partial U}{\partial t} = 0 = -\rho\frac{\partial\overline{u'w'}}{\partial z} + \mu\frac{\partial^2 U}{\partial z^2} = -\rho\frac{\partial}{\partial z}\left(\overline{u'w'} - \nu\frac{\partial U}{\partial z}\right) \qquad (4)$$

where $\nu = \mu/\rho$ is kinematic viscosity. Equations (3) and (4) demonstrate that the surface layer is a constant flux layer, where the total flux F_ψ, turbulent plus viscous, is independent of height. Introducing the eddy viscosity ν_t and eddy diffusivity K_ψ by analogy between turbulent and molecular diffusions,

$$\overline{u'w'} = -\nu_t\frac{\partial U}{\partial z} \;;\; \overline{w'\psi'} = -K_\psi\frac{\partial\Psi}{\partial z} \qquad (5)$$

the constant-flux equations (3) and (4) can be rewritten as

$$F_\psi = -\left(K_\psi(z) + D_\psi\right)\frac{\partial\Psi(z)}{\partial z} = F_{\psi s} = -u_*\psi_* \qquad (6)$$

$$\tau = +\rho\left(\nu_t(z) + \nu\right)\frac{\partial U(z)}{\partial z} = \tau_s = \rho u_*^2 \qquad (7)$$

where $F_{\psi s}$ and τ_s are the surface fluxes. Equations (6) and (7) also define the scaling variables u_* and ψ_*, independent of height. Away from the molecular sublayer, usually not thicker than 1 mm over the sea surface, $\nu \ll \nu_t(z)$ and $D_\psi \ll K_\psi$: the fluxes in (6) and (7) are actually the turbulent fluxes.

In the heat equation, the additional term S_h represents the influx of heat due to radiation and phase changes of moisture contained in the air. Equation (1) then reduces to

$$\rho C_p\frac{\partial T}{\partial t} = 0 = -\rho C_p\frac{\partial}{\partial z}\left(\overline{w'\theta'} - D_T\frac{\partial T}{\partial z}\right) + S_h \qquad (8)$$

where C_p is the specific heat of air at constant pressure.

Defining the additional vertical heat flux q_h by $S_h = -\partial q_h/\partial z$, *Monin and Yaglom* [1987] show that an equivalent relation to (7) can be written only when q_h is constant with height. As shown by these authors, the smallness of the variation with height of the vertical flux of radiant heat is not well assessed, but it is a usual assumption because of the difficulties to model radiation heating. In addition, in a layer where spray droplets are propelled, sensible and latent heat are exchanged with air at heights depending on the spray dynamics. As a consequence, the additional heat flux q_h is certainly not constant with height in atmospheric surface layer with evaporating spray, and S_h cannot be neglected as is usually done in the "constant flux layer."

In the same way, the evaporating droplets are elevated sources of moisture. Therefore an additional term is required in the budget equation of water vapor concentration ρ_v, which reads

$$\frac{\partial\overline{\rho}_v}{\partial t} = 0 = -\frac{\partial}{\partial z}\left(\overline{w'\rho_v'} - D_v\frac{\partial\overline{\rho}_v}{\partial z}\right) + S_v \qquad (9)$$

The budget equations for spray droplets can take different forms that depend on the parameter that represents aerosol concentration: total number concentration [*Ling and Kao*, 1976; *Stramska*, 1987], liquid water and salt mass concentrations [*Fairall and Edson*, 1989; *Fairall*, 1990], number concentration in size categories [*Ling et al.*, 1980; *Mestayer and Lefauconnier*, 1988], mass concentration in size categories [*Rouault et al.*, 1991], etc. In any case, the droplet budget includes not only an additional source term S_ψ representing the local influx of ψ due to phase changes (evaporation-condensation) but also flux terms representing the specific droplet dynamics: owing to inertia and weight, neither their mean nor their instantaneous velocities are equal to those of the air. Therefore the budget equation (1) keeps a general form,

$$\frac{\partial\Psi}{\partial t} = 0 = -W_\psi\frac{\partial\Psi}{\partial z} - \frac{\partial}{\partial z}\left(\overline{w_\psi'\psi'} - D_\psi\frac{\partial\Psi}{\partial z}\right) + S_\psi \qquad (10)$$

where $w_\psi = W_\psi + w_\psi'$ is a volume averaged vertical velocity component, whose definition depends on the choice of ψ.

If evaporation and condensation are the only physicochemical transformations taking place, then S_v is directly related to the droplet source term(s) S_ψ

$$S_v = \mathcal{F}(S_\psi) \qquad (11)$$

On the other hand, the source term in the heat equation (8) is composed of three parts

$$S_h = S_{hr} + S_{hs} + S_{hl} \qquad (12)$$

S_{hr} is the heat influx due to radiation, and S_{hs} is the heat influx due to the sensible heat exchange with droplets. This term arises because the droplets, generated at sea surface temperature T_{ss}, are rapidly propelled in air having a different temperature $T_a(z)$, and because they are never in thermal equilibrium with the surrounding air owing to evaporative cooling. S_{hl} is the heat influx due to the consumption/release of latent heat due to droplet evaporation/condensation. Most of the time, S_{hl} is a net sink in the heat budget, while S_{hs} can be either a sink or a source, depending on the air-sea temperature difference.

1.4 Recent Developments in Modeling Spray Behavior

In 1981, the Humidity Exchange Over the Sea Program (HEXOS) was initiated to study the water vapor and droplet fluxes from sea to air [*Smith et al.*, 1990]. The HEXOS studies In a Simulation Tunnel (HEXIST) part of the program was aimed at the development of numerical models to describe the turbulent

transport of evaporating droplets and their interactions with the scalar fields of temperature and humidity. Also, experimental simulations were performed for model validation purposes in the period 1985-1990 in the Large Air-Sea Interaction Simulation Tunnel of the Institut de Mécanique Statistique de la Turbulence (IMST) laboratory at Luminy (Marseille, France), and in the whitecap simulation tank at the University of Connecticut [e.g., *Mestayer et al.*, 1989].

The HEXIST program is a continuous cooperative framework for a progressive series of modeling efforts. Most of the resulting findings have been presented in the proceedings edited by *Mestayer et al.* [1990a] or in the review of *Andreas et al.* [1995]. Since the work presented in this paper takes advantage of the HEXIST efforts, a brief summary is presented below.

In IMST wind-water tunnel experiments the surface sources of droplets were provided by bubble plumes generated by immersed aeration devices, without breaking waves. The air flow was a well-known fully turbulent boundary layer over a flat water surface [*Mestayer et al.*, 1989; *Mestayer and Lefauconnier*, 1988]. Using the data obtained during these experiments, two numerical models were developed in parallel: a Lagrangian Monte Carlo model that calculates the trajectories of heavy evaporating droplets [*Edson*, 1989, 1990; *Edson and Fairall*, 1994; *Edson et al.*, 1996], and a Eulerian one-dimensional *K*-diffusivity model [*Rouault*, 1989; *Rouault et al.*, 1991]. In their initial stages, these models aimed at testing the basic modeling tools for turbulent dispersion and evaporation in two different numerical formulations, for the simplified configuration of the tunnel experiments: freshwater droplets from 5- to 100-μm radius in a fully developed laboratory boundary layer. The intercomparison of the two modeling efforts with the laboratory measurements demonstrated the feasibility of the two approaches and allowed for numerical optimizations of the turbulence models. The two models of droplet evaporation were based on *Pruppacher and Klett*'s [1978] equations for freshwater droplets, and demonstrated their efficiency. *Edson* [1989] also used these equations to show that the droplets under study reach very rapidly their thermal equilibrium owing to the combined effects of evaporative cooling and conductive heat exchange. This result was used by *Rouault et al.* [1991] to notably simplify the evaporation model of the Eulerian code by modeling droplet temperature by the local wet-bulb temperature T_{wb}.

With these models, *Rouault* [1989] and *Edson* [1990] assessed the droplet surface source function in the tunnel, also measured by *De Leeuw* [1988]. This source function was used by *Mestayer et al.* [1990b] and *Rouault et al.* [1991] to analyze the measurements of the humidity turbulence with a micro-Lyman-α hygrometer. These measurements showed a reduction of the turbulent flux of humidity $\overline{w'\rho_v'}$ in the lower part of the boundary layer, where the mean humidity $\overline{\rho}_v$ was increased by the droplet evaporation. The numerical simulations showed that the humidity increase, in the layer where the droplets evaporate, reduces the gradient of vapor concentration close to the surface and increases this gradient above the evaporation layer: this results in a simultaneous decrease of the turbulent flux of humidity at the water surface, and an increase of the flux in the higher layers that are not reached by the droplets. The net increase is therefore only a fraction of the vapor produced by the droplets (which is in turn only a fraction of the surface flux of (liquid) water). The theoretical consequences of this negative feedback were first analyzed by *Smith* [1990] and were also discussed by *Andreas et al.* [1995]. The simulations of *Mestayer et al.* [1990b] and *Rouault and Larsen* [1990] indicate that over a flat surface the thickness of the evaporation layer (where most droplets evaporate) is of the order of 1 or 2 m.

In parallel, *Andreas* [1989, 1990a] analyzed and simplified *Pruppacher and Klett*'s [1978] equations of the microphysics of aqueous solution drops, for their application to sea spray: his model equations describe the transient heat and mass exchanges of sea-spray water droplets with a constant atmospheric environment. A major result of his study is that air-droplet heat exchange is some 3 orders of magnitude faster than moisture exchange (a result extending *Edson*'s [1989] finding for freshwater droplets). One consequence is that the two processes can be modeled independently, as subsequently proposed by *Mestayer* [1990]. Another consequence is that all droplets, even large ones, have enough time to release sensible heat to the air during their flight. *Andreas* [1992] constructed a box model where air temperature and relative humidity are constant and droplets are introduced at sea surface temperature at a rate given by a surface source function extrapolated from the empirical function of *Miller* [1987]. The droplet heat and moisture exchanges are computed from *Andreas*'s [1989] equations, considering that the droplet residence time in the atmosphere box is

$$\tau_f = A_{1/3} / V_g(r) \tag{13}$$

where $A_{1/3}$ is the significant wave amplitude and $V_g(r)$ is the gravitational free-fall velocity (or terminal velocity) of a water sphere of radius r. The choice of $A_{1/3}$ to parameterize the droplet residence time, rather than the ejection heights measured by *Blanchard* [1963] (and recently by *Spiel* [1994]) or the evaporation layer thickness of *Mestayer et al.* [1990b] and *Rouault and Larsen* [1990], has been disputed by *Katsaros and De Leeuw* [1994], but it was reaffirmed by *Andreas* [1994].

Fairall et al. [1994] integrated the parameterizations of *Andreas* [1992] in a two-layer model in which the atmosphere box is replaced by an evaporation layer of thickness equal to $A_{1/3}$, that is topped by a classical constant-flux surface layer. The evaporation layer is a buffer where all air-spray exchanges of heat and moisture take place; this is equivalent to providing new "surface" conditions for an atmospheric surface layer over a virtual surface at $z = A_{1/3}$. The "virtual surface" fluxes are the sum of the sea surface fluxes, and of the droplet generated fluxes multiplied by a reduction factor α that models the negative feedback; a value of $\alpha = 0.5$ is deduced from the simulations of *Rouault and Larsen* [1990] and *Rouault et al.* [1991]. *Edson et al.*'s [1996] Eulero-Lagrangian simulations demonstrate that the value of this reduction factor depends dramatically on the initial behavior of the spray droplet, i.e., on the scale of the evaporation layer.

1.5 Nonlinear Issues

The models of *Andreas* [1992] and *Fairall et al.* [1994] showed that spray droplets can contribute noticeably to the heat and moisture budgets, provided that the source function is as modeled by *Andreas* [1992]. However, their box-type approach does not document the non-linear interaction processes generated by air-droplet exchanges at various heights in the lower atmosphere. The understanding of these near-surface processes is a key for the definitive assessment of the effective spray contribution. In tentative reconciliations between the below-up and above-down approaches to the surface source function, this problem seems to have been underestimated. The nonlinear processes can significantly reduce the spray contributions, and the net contributions may thus be much smaller than the potential

ones [*De Cosmo et al.*, 1995]; here "net" refers to the measurable effects over, e.g., the wave level (as in *Fairall et al.*'s [1994] two-layer model), while "potential" represents the maximum heat and moisture droplets could exchange with air as approached by *Andreas*' [1990a] model. For instance, *Andreas* [1992] and *Andreas et al.* [1995] stress that the potential sensible heat transfer from droplets to air should not be neglected, since it can be very large, eventually as large as the surface flux. On the other hand, *Andreas* [1989, 1992] demonstrated that drop-to-air heat transfer is extremely rapid, faster than a second. One possible explanation is that the sensible layer, where air-spray sensible heat transfers take place (equivalent to the evaporation layer) is very thin and lies immediately over the surface: by following *Smith*'s [1990] and *Andreas et al.*'s [1995] description of the negative feedback it might then seem natural to conclude that this heat transfer is almost exactly compensated by the altered surface transfer due to the altered temperature gradient in this thin layer ... and that its net effect would then be null or negligible. This example shows how nonlinear interactions could be difficult to predict. We think that it is dangerous to draw conclusions too rapidly without models that explicitly handle the nonlinear interactions. Also, a better assessment of the initial dynamics of spume droplets is needed.

A major assumption in the recent derivations of the spray surface source function is that $\partial F/\partial r$ has the same dependence on r as that observed in the measured droplet concentrations [*Monahan et al.*, 1986]. As the bubble-mediated component of $\partial F/\partial r$ is most certainly proportional to the number of bubbles entrained in water, which is in turn proportional to the whitecap coverage, this assumption extends the proportionality to the whole droplet spectrum, in which case it is possible to write $\partial F/\partial r$ under the form

$$\frac{\partial F}{\partial r}(r,U) = \mathcal{W}(U)\ \frac{\partial f}{\partial r}(r) \qquad (14)$$

where $\partial f/\partial r$ is the wind-independent source function per unit area of whitecap and $\mathcal{W}(U)$ is either the fractional coverage of stage B whitecaps $\mathcal{W}_B(U) \propto U_{10}^{3.41}$ [*Monahan et al.*, 1986] or the efficient whitecap coverage of *Miller and Fairall* [1988] $\mathcal{W}_{ef}(U) \propto U_{10}^{2.22}$ (as computed by *Andreas* [1990b]). On the other hand, *Andreas et al.* [1995] speculate that the bubble-mediated component of $\partial F/\partial r$ is proportional to the wind-to-sea energy transfer rate and thus should vary as u_*^3 (or $\sim U_{10}^{4.5}$) while the spume component should vary "somewhat slower than u_*^3."

Recently, *Smith et al.* [1993] measured concentrations of droplets from 2 to 25 μm at one fixed height (z = 14 m) over a very large range of wind speeds (0-30 m s^{-1}). They deduced the droplet fluxes, using *Slinn and Slinn*'s [1981] modeled particle deposition velocities (i.e., equating upward and downward fluxes at z = 14 m). Their fluxes appear to vary with $U^{2.6}$ for the smaller droplets ($r \sim 2$ μm) generated by bubbles only and with U^5 for larger droplets ($r \sim 20$ μm) mixing jet and spume origins. The relatively good agreement with *Monahan et al.*'s [1986] below-up surface fluxes for the smaller droplets seems to indicate that a large part of those do reach the height of 14 m. As noted by the authors, their large-droplet flux estimations at this height cannot be used for conclusive comparisons with below-up surface flux estimations since they do not have the proper model for large droplet behavior.

Therefore the proportionality assumption expressed by Equation (14) should be re-analyzed from three points of view.

1. As already noted by *Monahan et al.* [1986], if relation (14) is valid for the bubble-mediated component, how can it be valid for the whole spectrum if the spume component has a different wind dependency [*Fairall et al.*, 1994] ?

2. Considering the differences in the dispersion of droplets close to the surface due to their different weights, inertia, and size variations that depend on wind speed, should the below-up source function present the same radius dependency as the above-down "effective" functions deduced from concentration measurements by implicitly neglecting the surface-induced motions [*Wu*, 1989, 1990, 1993] ?

3. Is the proportionality assumption consistent with a two-layer model where practically all droplets are assumed to evaporate in the lower layer, below $z = A_{1/3}$ [*Fairall et al.*, 1994] ?

Other nonlinear issues of importance are the droplet residence time, the thickness and the structure of the evaporation and heat exchange layers, their overall efficiency to transfer the droplet contributions upward, the resulting net distributions of upward dispersed aerosol, and their variations with wind speed and meteorological conditions.

The Couche Limite Unidimensionnelle Stationnaire d'Embruns (CLUSE) model of *Rouault et al.* [1991] proved to be a good basis for studying the nonlinear interaction between injection, evaporation, turbulent diffusion and transport of spray droplets [*Mestayer*, 1990; *Rouault et al.*, 1991]. However, since it was developed for artificial conditions in a wind-wave interaction tunnel (see above), the CLUSE model must be extended to open ocean conditions before it can describe the behavior of sea spray droplets. This extension to the new code SeaCluse is described in the next section. Since this paper focuses on the droplet dynamics, the implementation of *Mestayer*'s [1990] model of seawater droplet evaporation and its results are not presented here and will be analyzed separately in a sequel paper. As shown below, the development of SeaCluse required creating a "preprocessor" for computing mean air flows and droplet trajectories over the waves: this preprocessor is described in section 3, and the results obtained during the preliminary simulations are analyzed in the context of the above discussions. In section 4, three models of droplet turbulent diffusivity are presented and the resulting distributions of the dispersed droplets are analyzed. Finally, section 5 presents some provisional conclusions on some nonlinear issues and suggests fruitful lines for cooperative works.

2. The Model

2.1 Model Bases

The family of CLUSE-derived numerical codes are Eulerian one-dimensional average codes computing the stationary distributions of droplet concentrations along a vertical axis over the water surface. The heart of the codes is the computation of the coupled stationary budget equations of interacting transportable quantities by a finite volume solver (micro-integral method, see *Schiestel* [1993]). The framework of this model family is defined by the following basic hypotheses.

1. The fluid is incompressible.
2. The Coriolis force is negligible.
3. The Boussinesq approximations may be applied.
4. The droplets are spherical and do not breakup or coalesce.
5. The total number of droplets in the domain of study is conserved.
6. The boundary layer is fully developed, and the classical horizontal homogeneity hypothesis is applied. The constant flux hypothesis can be used in the whole domain for the transportable variables that have no local source.

7. The total mass of droplets is too small to noticeably influence the dynamics of air.

8. The molecular sublayer is not under study, and the effect of molecular diffusivity is negligible, compared to the other fluxes.

The fluid is considered to be a multiphase mixture of $N+2$ components: dry air, with concentration ρ_a, water vapor with concentration ρ_v, and N droplet categories of nominal radius r_n ($n = 1, ..., N$) and concentration ρ_n. Category n includes all droplets of radius r defined by:

$$r_n - \Delta r_n/2 < r \le r_n + \Delta r_n/2 \qquad (15)$$

Mass concentrations per unit volume ρ_a, ρ_v, and ρ_n are considered rather than humidity and number density because these are the transportable conservative variables.

The instantaneous budget equation of mass of any of the $N+2$ transportable components is

$$\frac{\partial \rho_\gamma}{\partial t} + \frac{\partial\left(\rho_\gamma V_{\gamma j}\right)}{\partial x_j} = S_\gamma \quad \gamma = a, v, n;\ n = 1, ..., N \qquad (16)$$

where $V_{\gamma j}$ is the velocity component in direction j of the component γ and S_γ is the algebraic sum of all local sources of ρ_γ.

Reynolds decomposition is introduced as in (2), and relations (16) are averaged. Because of the horizontal homogeneity hypothesis, the flux divergences in the x and y directions are null. The velocity components $V_{\gamma j}$ are replaced by their usual notations $V_{\gamma x} = U_\gamma$ and $V_{\gamma z} = W_\gamma$.

For the gas phase components, dry air and water vapor, $V_{\gamma j}$ is equal to the velocity of air $V_{a j}$. Because of hypotheses 2, 6, and 7, $\overline{W_a} = 0$. For particle concentrations, $V_{n j}$ is the average of the velocities of the particles of category n contained in the elementary volume under consideration. Owing to their initial ejection from the surface and their further gravitational attraction, $\overline{W_n} \neq 0$. Owing to their inertia, $w_n' \neq w_a'$. The basic equations of the models are the averaged budget equations for the concentrations and the specific heat, deduced from (16) and written as:

$$\underset{1}{\frac{\partial \overline{\rho_a}}{\partial t}} = 0 \qquad (17a)$$

$$\underset{1}{\frac{\partial \overline{\rho_n}}{\partial t}} = \underset{2}{-\frac{\partial\left(\overline{\rho_n}\,\overline{W_n}\right)}{\partial z}} \underset{3}{-\frac{\partial\left(\overline{\rho_n' w_n'}\right)}{\partial z}} + \underset{4}{S_n} \qquad n = 1, ..., N \qquad (17b)$$

$$\underset{1}{\frac{\partial \overline{\rho_v}}{\partial t}} = \underset{3}{-\frac{\partial\left(\overline{\rho_v' w_a'}\right)}{\partial z}} + \underset{4}{S_v} \qquad (17c)$$

$$\underset{1}{\rho_a C_{pa} \frac{\partial \overline{T}}{\partial t}} = \underset{3}{-\rho_a C_{pa} \frac{\partial\left(\overline{T' w_a'}\right)}{\partial z}} + \underset{4}{S_h} \qquad (17d)$$

Terms 1 represent the time variations of the transported quantities, which tend toward zero in stationary conditions. Terms 2 represent the macroscopic fluxes due to ejection of droplets from the surface and their gravitational fall. Terms 3 represent the diffusion due to turbulence. Terms 4 are the local source-sink terms. The solution of the system of coupled stationary equations is found by an iterative process where, at each time step, equations (17b)-(17d) are computed over the whole computation domain, up to equilibrium when terms 1 equal 0 [see *Rouault et al.*, 1991].

Since the SeaCluse model is built by extending the CLUSE model from simple theoretical/laboratory conditions to more realistic and complex marine conditions, it is convenient to first briefly describe the original model and then concentrate on the extensions.

2.2 Original CLUSE Model

The CLUSE model of *Rouault* [1989] and *Rouault et al.* [1991] considers freshwater jet droplets between 5 and 105 μm in radius, ejected from the water surface by bursting bubbles. The model is to be tuned by an experimental surface source function. The droplets are then dispersed by turbulence in a fully developed boundary layer over a flat air-water interface. The diffusion by air turbulence is represented by a K diffusivity term, and gravitational and inertial effects are explicitly modeled. The droplet population is split into size bins (categories). Each droplet category is allowed to interact with the ambient humid air; source-sink functions in the budget equations represent the effects of droplet evaporation: transfer between droplet categories due to shrinking, production of water vapor and absorption of sensible heat.

The boundary conditions are those of a theoretical atmospheric surface layer: T and ρ_v are prescribed at the upper and lower boundaries with $\rho_v(z_{min}) = \rho_{v\,surf} = \rho_{v\,sat}(T(z_{min}))$, where $\rho_{v\,sat}(T)$ is the saturation vapor concentration at temperature T computed by means of *Buck*'s [1981] formula. The upper boundary is set high enough to ensure that the droplet flux is zero. At the lower boundary the droplet flux is prescribed from the algebraic sum of an upward flux of injected spray and a downward flux of falling/depositing droplets. The upward flux is prescribed from the experimental surface source function, while the downward flux is obtained at each time step by integrating Equation (17b) over the whole computation domain (Hypothesis 5).

The turbulence terms 3 in (17) are modeled by means of exchange coefficients, assuming a classical variation of the eddy viscosity $\nu_f(z) = \kappa u_* z$ (where κ is von Karman's constant, $\kappa = 0.4$) and by explicitly modeling the reduction of droplet diffusion by turbulence due to inertia (this will be discussed in detail in section 4).

Terms 2 in (17b) represent the macroscopic fluxes due to ejection of droplets from the surface and their gravitational fall. Rather than computing budget equations for the macroscopic fluxes $\overline{\rho_n}\,\overline{W_n}$ (with disputable closure assumptions), *Rouault et al.* [1991] modeled these terms by relaxation terms of the form

$$\frac{\partial\left(\overline{\rho_n}\,\overline{W_n}\right)}{\partial z} = \frac{1}{C_1 T_{fly,n}}\left[\overline{\rho_n}(z) - \rho_n^o(z)\right] \qquad (18)$$

where $T_{fly,n}$ denotes the flight time of the droplets and $\rho_n^o(z)$ their concentration in nonturbulent and nonevaporative conditions. The constant C_1 was adjusted by *Rouault* [1989] to 0.75 by comparison with experimental data obtained in the IMST simulation tunnel.

Finally, terms 4 in (17) represent the sources due to droplet evaporation. Within the hypothesis of conservation of the total number of droplets, *Mestayer and Lefauconnier* [1988] formulated the relationship between S_n, the droplet spectrum $\rho_n(r)$, and the mass rate of change of an isolated droplet $\dot{m}_n$

$$S_n = 6\rho_n \frac{\dot{r}_n}{r_n} - \dot{r}_n\left(\frac{\partial \rho_n(r)}{\partial r}\right)_{r_n} - \rho_n\left(\frac{\partial \dot{r}}{\partial r}\right)_{r_n} \qquad (19)$$

where $\dot{r}_n = (dr/dt)_{r_n}$ and $\dot{m}_n = (dm_d/dt)_{r_n} = 4\pi \rho_w r_n^2 \dot{r}_n$. In CLUSE $\dot{m}_n$ is described by a simplified version of *Beard and Pruppacher*'s [1971] model of an evaporating droplet falling at terminal velocity, which also gives good results for evaporating droplets in a turbulent flow [*Edson and Fairall*, 1994]. In this version, fresh water is considered and the droplet surface temperature is assumed equal to the wet-bulb temperature of the surrounding air. Since evaporation is the only considered transformation,

$$S_v = -\sum_{n=1}^{N} S_n \quad ; \quad S_h = -L_v S_v \qquad (20)$$

where L_v denotes the latent heat of evaporation.

2.3 SeaCluse Model

Since most of the air-droplet exchange processes take place close to the sea surface, the calculation domain extends now from the wave troughs to the top of the atmospheric surface layer. Special treatments are required to model the levels between wave troughs and crests, since they correspond to regions alternately occupied by air, water, and the surface. The terms of the modeled equations must represent the effects of the various processes averaged over the fraction of time these levels are occupied by air. The intermittent presence of the surface at these levels is modeled by additional elevated source terms. Also, the model uses several prescribed functions as $v_f(z)$ and $\rho_n^o(z)$. This last function requires computing trajectories of nonevaporating droplets in the absence of turbulent diffusion.

The extension of CLUSE to SeaCluse thus requires three basic developments: (1) a module for computing the prescribed vertical profiles, based on a model for the mean air flow over the waves; this module is called the "mean field preprocessor," its calculations being independent of the use of the results in the "main program"; (2) an evaporation module for seawater droplets; and (3) a surface source function including jet and spume droplets. In addition, the extension to open ocean of the turbulent diffusion models must be assessed.

The evaporation of saltwater droplets is treated in the way that was previously presented by *Mestayer* [1990]. Saltwater evaporation differs from fresh water, not only quantitatively but also because the droplets can only shrink to a minimum size of local equilibrium determined by their salt content and the ambient relative humidity. This changes not only the rate at which the water vapor is released but also, consequently, the height where it is released.

In its present state, the SeaCluse code considers open ocean conditions where the wave field is in equilibrium and moves in the same direction as the wind. It is important to keep in mind that the SeaCluse model is a 1-D Eulerian model (height only) and that it does not deal with the coordinates x and y. This can be visualized by an observer who remains fixed at a certain position x and watches the waves go by. The waves induce changes in the values of $U(z)$, $T(z)$, $\rho_v(z)$, etc. Since the model calculates a stationary solution, the observer cannot specify these variables as a function of time. Therefore they have to be averaged over the waves. The wave field is represented by a fifth-order Stokes wave [*Donelan and Hui*, 1990], whose amplitude H_o and period T_w are prescribed as a function of wind speed (see Figure 1 and section 3). As a consequence, the mean variables like $U(z)$ vary periodically in time with the same period, and it suffices to average over a time $t = T_w$. This can also be seen in a co-ordinate system that moves along with the wave with the phase velocity C_w,

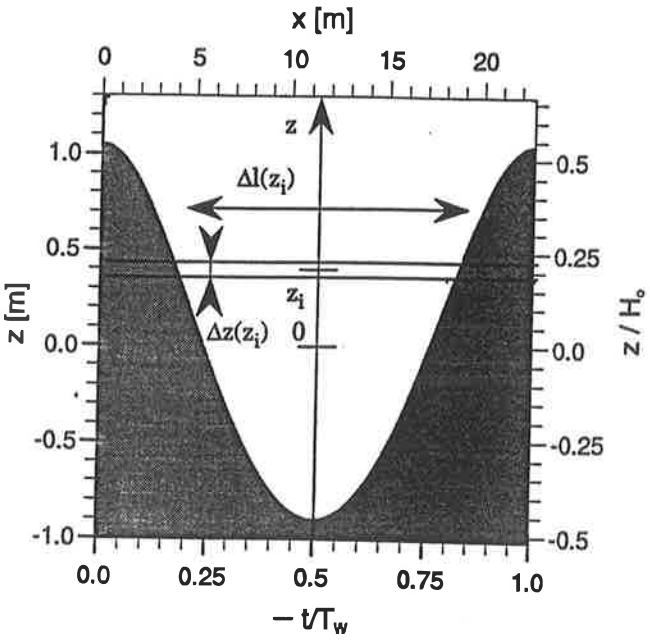

Figure 1. The wave surface in the preprocessor

where the position of the wave surface does not move: its elevation η is $\eta(x,t) = \eta(x)$ (see section 3). Therefore SeaCluse includes implicitly the model of the air flow over the wave field that is explicitly computed in the preprocessor: the model in SeaCluse is the average of the model in the preprocessor.

The calculation domain extends from $z_{min} = -H_o/2$, where $z = 0$ corresponds to mean sea level, to an arbitrary upper limit z_{max}. In all the computations presented here this limit is fixed at $z_{max} = 100$ m, and the top boundary conditions are those of an open atmospheric surface layer: constant fluxes, with $\rho_n(z_{max}) = 0$ and $T(z_{max})$ and $\rho_v(z_{max})$ fixed to their initial values actually deduced from T_{10} and ρ_{v10}, the values at the reference height of 10 m AMSL (see section 3). The condition of zero droplet fluxes is actually not imposed but only checked during the simulations. This assumes that most of the air-droplet exchanges take place in the lower part of the atmospheric surface layer and that the layer above does present the characteristics of a Monin-Obukhov constant-flux layer. If the condition is not well verified, e.g. in the case of a very low inversion, then the present boundary conditions need be replaced by conditions representing an entrainment layer. The conditions at the lowest boundary ($z = -H_o/2$) are the following: $T = T_{ss}$, $\rho_v = \rho_{vss} = \rho_{v\,sat}(T_{ss})$, $\rho_n = 0$ (see below).

The turbulence terms 3 of (17) are modeled in a way relatively similar to that of the original CLUSE model (see section 4). The terms 2 in (17b) are modeled as in (18), but the computation of $T_{fly,n}$ and $\rho_n^o(z)$ is more complicated over a wavy surface. Over a flat surface they are obtained by computing the ballistic trajectory of one droplet of radius r_n whose initial ejection velocity V_e is matched to *Blanchard*'s [1963, 1989] data (see section 3). In the absence of turbulent diffusion, the vertical projection of the trajectory is independent of the wind speed and is therefore computed with zero horizontal wind. Here $\rho_n^o(z)$ is proportional to the droplet time of presence at level z, i.e.,

$$\rho_n^o(z) \propto \left(\left| W_n^{up}(z) \right|^{-1} + \left| W_n^{down}(z) \right|^{-1} \right) / T_{fly,n} \qquad (21)$$

and proportional to the surface source function $dF(r_n)/dr$. The distribution of $\rho_n^o(z)/(dF(r_n)/dr)$ is therefore a function of r_n

only, computed once for a given computational grid. Over the wavy surface, the droplet trajectories depend not only on the droplet size but also on the wave shape, the wind speed, and the initial position of the droplet at ejection. $T_{fly,n}$ and $\rho_n^o(z)$ must therefore be computed for each run by averaging the flight times and times of presence at level z of a series of droplets of radius r_n ejected from various positions along the wave profile with the same initial ejection velocity $V_e(r_n)$. This is done by the mean field preprocessor (see section 3.3).

The source terms 4 of (17) include the effects of air-droplet exchanges and the intermittent presence of the surface at level z:

$$S_n(z) = E_n(z) + G_n(z) + D_n(z) \tag{22}$$

The exchange source function $E_n(z)$ is similar to (19). The droplet generation source function $G_n(z)$ expresses the "creation" of mass in a grid mesh located between $-H_o/2$ and $+H_o/2$ due to the upward flux of droplets through the elements of the surface that are between $z - dz(z)/2$ and $z + dz(z)/2$. It is expressed by

$$G_n(z) = \rho_n^e \, W_n^e \, \phi_n^e(z)/dz \tag{23}$$

where $\rho_n^e W_n^e$ is the bulk droplet surface flux ejected from the surface (see below), and $\phi_n^e(z)$ is a distribution function deduced from the wave profile geometry, the grid mesh distribution, and the distribution of the sources of droplets along the wave surface (e.g., jet drop sources are homogeneously distributed, but spume drop sources are distributed in the vicinity of wave crest only).

The droplet deposition source function $D_n(z)$ expresses the sink of mass in a grid mesh located between $-H_o/2$ and $+H_o/2$ due to the downward flux of droplets depositing on the surface elements. It is expressed by

$$D_n(z) = \rho_n^d(z) \, W_n^d \, \phi_n^d(z)/dz \tag{24}$$

where $\rho_n^d(z) W_n^d$ is the mass flux of droplets of category n depositing on the surface elements and $\phi_n^d(z)$ is another distribution function. Here, $\phi_n^e(z)$ and $\phi_n^d(z)$ are defined from $-H_o/2$ to $+H_o/2$ and equal to 0 higher, with

$$\int_{-H_0/2}^{H_0/2} \phi_n^e(z)dz = \int_{-H_0/2}^{H_0/2} \phi_n^d(z)dz = 1 \tag{25}$$

In the "main program" the parameters in (23)-(24) are obtained in the following way. The computational grid is defined from $i = 1$ to IMAX, and the first grid mesh is chosen such as to include a portion of the surface ($z_{min} = -H_o/2$) but no portion of air, making it possible to write the boundary condition $\rho_n(z_{min}) = 0$. In the discrete form of (23)-(25), dz is replaced by $\Delta z(z_i)$, the thickness of the ith computational grid mesh centred at level $z_i = z$ and the distribution functions ϕ_n^e and ϕ_n^d by f_n^e and f_n^d. Since the droplet deposition is expected to be homogeneously distributed along the surface, $f_n^d(z_i)$ is the relative length of the surface elements intersected by the ith grid mesh:

$$f_n^d(z_i) = \frac{2\Delta z(z_i)}{\lambda} \Big/ \frac{\partial \eta}{\partial x}(z) \qquad -H_o/2 \le z \le H_o/2$$
$$f_n^d(z_i) = 0 \qquad z > H_o/2$$
$$\text{with} \sum_{i=1}^{IMAX} f_n^d(z_i) = 1 \tag{26}$$

where $\partial\eta/\partial x$ is the wave slope and λ the wavelength (see section 3.1); while $f_n^e(z_i) = f_n^d(z_i) \, f_n^s(z_i)$, where $f_n^s(z_i)$ is the prescribed distribution of the droplet sources, with

$$\sum_{i=1}^{IMAX} f_n^e(z_i) = 1.$$

$G_n(z)$ is constant, while the other source terms are computed at each time step. In (23), $\rho_n^e W_n^e$ is obtained from dF/dr. The prescribed surface source function dF/dr is the number of droplets ejected per m^2, per second, per micron radius increment (m^{-2} s^{-1} µm^{-1}). The droplets are ejected at the initial velocity $W_n^e = V_e(r_n)$ (m s^{-1}). Therefore the source mass flux is

$$\rho_n^e W_n^e = \left(\tfrac{4}{3}\pi r_n^3 \rho_w\right) \frac{dF}{dr} \Delta r_n \tag{27}$$

where ρ_w is the density of water and Δr_n is the width of the radius bin: Δr_n is in µm, r_n in m, ρ_w and ρ_n^e in kg/m^3. In (24), W_n^d is modeled by the average final fall velocity of droplets n, $W_n^d = V_f(r_n)$, obtained from the preprocessor calculations of droplet trajectories without evaporation and turbulent diffusion (see section 3.3). Here, $\rho_n^d(z_i)$ is the mass of droplets n that depose on the elements of surface intersected by the grid mesh: it is proportional to the mass of droplets n that is present in the mesh and inversely proportional to the length of air that is "contained" in the mesh (see Figure 1):

$$\rho_n^d(z_i) = \alpha_n \rho_n(z)/\Delta l(z_i) \tag{28}$$

The proportionality constant α_n (in meters) is independent of z, but it is computed at each time step to ensure conservation of mass. This is done by computing the budget of the category n over the whole calculation domain, which reduces to

$$\int_{z_{min}}^{z_{max}} \left[-\frac{\partial\left(\overline{\rho_n}\,\overline{W_n}\right)}{\partial z} - \frac{\partial\left(\overline{\rho_n' w_n'}\right)}{\partial z} + S_n(z) \right] dz = \int_{z_{min}}^{z_{max}} S_n(z)\, dz = 0 \tag{29}$$

since the integrals of the vertical transfer terms amount to zero, because of the choice of the first grid mesh and hypothesis 5. In discrete form, this reads

$$\sum_{i=1}^{IMAX} E_n(z)\Delta z(z_i) + \left(\rho_n^e W_n^e\right) \sum_{i=1}^{IMAX} f_n^e(z_i) + \alpha_n V_f(r_n) \sum_{i=1}^{IMAX} \rho_n(z) f_n^d(z_i)/\Delta l(z_i) = 0$$

or

$$\alpha_n = -\frac{1}{V_f(r_n)} \frac{\rho_n^e W_n^e + \sum_{i=1}^{IMAX} E_n(z)\Delta z(z_i)}{\sum_{i=1}^{IMAX} \rho_n(z) f_n^d(z_i)/\Delta l(z_i)} \tag{30}$$

The source of water vapor mass is obtained from the loss of liquid water mass:

$$S_v(z) = -\sum_{n=1}^{N} E_n(z) \tag{31}$$

The source term in the equation of specific heat of air is composed of two parts corresponding to the sensible and latent heat exchanges with the droplets:

$$S_h(z) = H_S(z) + H_L(z) \tag{32}$$

This equation does not include a third term for the influx due to radiation, since it would complicate the simulations and would not furnish additional information about air-spray interactions.

The latent heat term is the sink of heat lost by air to evaporate the droplets

$$H_L(z) = -L_v S_v(z) = L_v \sum_{n=1}^{N} E_n(z) \tag{33}$$

$H_S(z)$ represents the sensible heat exchange between air and droplets. Its modeling is still in progress. Since it is not used in the simulations that are presented here, its detailed description is postponed to a further publication.

3. The Mean Field Preprocessor

3.1 Wave Model

In this section we discuss the two-dimensional model (2-D) of the air flow over the waves and the trajectories of droplets in the absence of turbulence that are used to compute the parameters and reference vertical profiles that are prescribed in SeaCluse.

Our aim is to develop a code that requires as inputs only the standard micro-meteorological parameters: wind speed, humidity, air temperature, and sea surface temperature. The key input is U_{10}, the wind speed at a reference height of 10 m: it directly determines the friction velocity, and the amplitude and frequency of the waves. The friction velocity is computed from the "bulk formula"

$$u_*^2 = -\overline{u'w'} = C_D U_{10}^2 = C_{DN} U_{10N}^2 \tag{34}$$

where C_{DN} is the reference drag coefficient in neutral condition, that depends on U_{10} and wave state, that in turn, depends on the wind speed and direction, the water depth, the fetch, the wave field "history," etc. (see *Geernaert* [1990] for an overview). On the open ocean, with a fully developed equilibrium wave field, C_{DN} is given by [*Smith*, 1980, 1988]

$$10^3 C_{DN} = 0.61 + 0.063 U_{10} \tag{35}$$

In practice, u_* is obtained either by computing the value of C_D from

$$C_D^{1/2} = C_{DN}^{1/2} \left[1 - C_{DN}^{1/2} \Psi_u(z/L)/\kappa\right]^{-1/2} \tag{36}$$

where Ψ_u is the profile stability function [*Panofsky and Dutton*, 1984] or by obtaining U_{10N} from (50), as described in the next section.

The wave field is described by a fifth-order Stokes wave. Although this is not a good representation of the wave field in the presence of breaking waves, it is assumed that this analytical representation will provide a good enough framework for computing a mean air flow field and that the averaged vertical profiles of turbulent diffusivity and droplet concentrations over the wavy surface do not depend much on the exact shape of the wave. The fifth-order Stokes wave can be seen either as a 2-D stationary wave in the (x,z) plane (i.e., infinite in the direction normal to the wind) in a frame of reference traveling at the wave celerity C_w:

$$\eta(x,t) = \eta(x) = k^{-1} \sum_{j=1}^{5} \beta_j(h) \cos(jkx) \tag{37}$$

or as a time-dependent surface elevation in the 1-D space of SeaCluse:

$$\eta(x,t) = \eta(t) = \left(C_w/\omega\right) \sum_{j=1}^{5} \beta_j(h) \cos(-j\omega t) \tag{38}$$

where [e.g., *Donelan and Hui*, 1990]:

$$\begin{aligned}
\beta_1 &= h - \frac{3}{8}h^3 - \frac{211}{192}h^5 \\
\beta_2 &= \frac{1}{2}h^2 + \frac{1}{3}h^4 \\
\beta_3 &= \frac{3}{8}h^3 + \frac{99}{128}h^5 \\
\beta_4 &= \frac{1}{3}h^4 \\
\beta_5 &= \frac{125}{384}h^5
\end{aligned} \tag{39}$$

The Stokes parameter h defines the average wave slope or steepness,

$$h = k H_o/2 = \pi \frac{H_o}{\lambda} = \pi \frac{H_o}{C_w T_w} \tag{40}$$

where H_o is the trough-to-crest height, k the wave number, λ the wavelength, T_w the wave period ($\lambda = C_w T_w$) and $\omega = 2\pi/T_w$. The Stokes wave celerity is given by

$$C_w^2 = \frac{g}{k}\left(1 + h^2 + h^4/2\right) \tag{41}$$

while its wave age Γ is defined by

$$\Gamma = C_w/U_{10} \tag{42}$$

Most of the present simulations use the value of the Stokes parameter $h = 0.135$ observed by *Janssen et al.* [1989], and the value of the wave age for a fully developed wave field, $\Gamma = 0.85$ [*Geernaert*, 1990] (Figure 1).

Obviously, the assumption of fully developed waves will often be violated in coastal regions [e.g., *Maat et al.*, 1991] and a fetch-dependent model is also being developed for those situations [*Mestayer*, 1991].

3.2 Mean Air Flow Model and Vertical Profiles

The SeaCluse assumption 5 considers that the air dynamics is not influenced by the presence of the droplets because their total momentum is negligible with respect to that of air. To calculate the vertical profiles, the calculation domain is split into two regions: the wave region, where the waves influence the air flow, and the upper region, where the waves do not influence the air flow.

The structure of the upper region is that of a classical turbulent boundary layer over a flat surface, i.e., an atmospheric surface layer where the eddy viscosity ν_t is given by

$$\nu_t(z) = \kappa u_* z/\varphi_u(z/L) \qquad z > H_o \tag{43}$$

where $\varphi_u(z/L)$ takes into account the influence of thermal stability (see below). L is the Monin-Obukhov length, defined by

$$\frac{z}{L} = \frac{g}{T_o} \frac{\overline{w'T'} + 0.61 T \overline{w'\rho_v'}/\rho_a}{-u_*^3/(\kappa z)} \tag{44}$$

In the wave region the assumption of a fully developed wave field makes it possible to further assume that momentum is only transferred to the water and not to the waves. Considering that local surface slopes have small values, it is therefore natural to assume that the structure of the mean flow is locally that of a turbulent boundary layer over a flat surface. Of course, this assumption is limited to conditions when the mean wave profile is not

very steep, so that there is no air flow separation at the crest. In that case, local profiles $\nu_t(z,t)$ may be calculated by

$$\begin{aligned} \nu_t(z,t) &= \kappa\, u_* \left[z-\eta(t)\right]/\varphi_u(z/L) && \eta(t) < z < H_o \\ \nu_t(z,t) &= 0 && -H_o/2 < z < \eta(t) \end{aligned} \quad (45)$$

where $\eta(t)$ corresponds to the height of the wave surface at time t. The average profile $\nu_t(z)$ in the wave region is calculated by

$$\nu_t(z) = \overline{\nu_t(z,t)} = \frac{2}{T_w}\int_0^{T_w/2} \nu_t(z,t)\, dt \qquad -H_o/2 < z < H_o \quad (46)$$

where it suffices to integrate over half a wave period because of symmetry.

It has been reported that the wave region, where the waves influence the air flow, extends up to 5-10 times H_o (the wave crest is at $z = H_o/2$). However, when constructing the profile of ν_t with (41)-(46), above $z = H_o$ there is no visible difference between the average of the local profiles and the atmospheric ν_t. Figure 2 shows the resulting profiles of $\nu_t(z)$ for $U_{10} = 10$ and 20 m/s (the dashed curves are discussed at the end of this subsection). The net effect of the wave surface integration is that the slope of $\nu_t(z)$ is decreased, and consequently $\nu_t(z) = 0$ is reached below $z = 0$. The number of local profiles that are averaged is not very important: a minimum of 20 is required, but averaging more profiles yields essentially the same results.

With the hypothesis that the constant flux assumption is valid for momentum in the upper region, the wind profile may be calculated from $\nu_t(z)$ by the "flux-gradient relationship," i.e., by inverting (5):

$$\frac{\partial U}{\partial z} = \frac{u_*^2}{\nu_t(z)} = \frac{u_*}{\kappa z}\varphi_u(z/L) \qquad z > H_o \quad (47)$$

where the atmospheric stability function φ_u is [*Edson et al.*, 1991]

$$\begin{aligned} \varphi_u(z/L) &= (1-20\, z/L)^{-1/4} && z/L \le 0 \\ \varphi_u(z/L) &= 1+8\, z/L && z/L \ge 0 \end{aligned} \quad (48)$$

The initial value of z/L is obtained by means of the bulk aerodynamic formula of *DeCosmo et al.* [1995]:

$$\begin{aligned} -\overline{T'w'} = u_* T_* &= C_H\left(T_{10}-T_{ss}\right)U_{10N} && C_H = 1.0\cdot 10^{-3} \\ -\overline{\rho_v' w'} = u_* \rho_{v*} &= C_E\left(\rho_{v10}-\rho_{vss}\right)U_{10N} && C_E = 1.2\cdot 10^{-3} \end{aligned} \quad (49)$$

where the "neutral" U_{10N} is defined below. In simulations of real experiments, the value of z/L must be readjusted after a complete computation of the SeaCluse model has furnished the actual fluxes of heat and moisture, including the droplet induced fluxes. This implies reiteration of the calculation. In the present simulations neutral conditions are used.

Using (47), the wind profile is constructed from the reference level $z = 10$ m where $U(10) = U_{10}$, up to the top of the domain and down to $z = H_o$. The wind profile thus obtained is used to infer an important parameter for the modeling of turbulence, the roughness length z_{ou}, by a regression to fit the wind profile to

$$U(z) = \frac{u_*}{\kappa}\left[ln\left(z/z_{ou}\right) - \psi_u(z/L)\right] \qquad z > H_o \quad (50)$$

where the profile stability function ψ_u is obtained from φ_u [see *Panofsky and Dutton*, 1984; *Geernaert*, 1990]. This also makes it possible to obtain $U_{10N} = Ln(10/z_{ou})\, u_*/\kappa$.

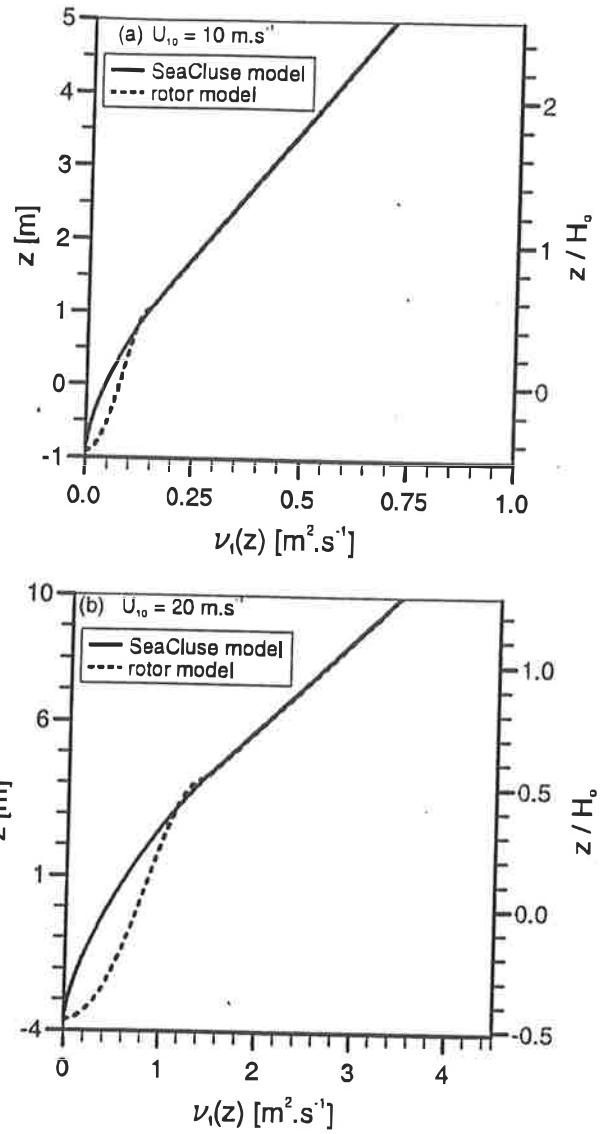

Figure 2. Average eddy viscosity profile for (a) $U_{10} = 10$ m/s and (b) $U_{10} = 20$ m/s.

The wind profile in the wave region is calculated as a function of the surface elevation $\eta(x,t) = \eta(t)$. In that case, "local" logarithmic profiles $U(z,t)$ are given by

$$U(z,t) - u_{0L}(t) = \frac{u_*}{\kappa} ln\left(\frac{z-\eta(t)}{z_{oL}(t)}\right) \qquad \eta(t) \le z < H_o \quad (51)$$

where $u_{0L}(t)$ denotes the local value of $U(z,t)$ at the wave surface, $u_{0L}(t) = U(\eta(t),t)$, and $z_{oL}(t)$ is a free parameter identical to a "local" roughness length. The wind speed at the surface is composed of a local component due to the orbital motion of the water and a constant component due to surface slip. These components are approximated by

$$u_{0L}(t) = U\left(\eta(t),t\right) = \omega\eta(t) + \kappa u_* \quad (52)$$

The values of $z_{oL}(t)$ are obtained by imposing the condition that all local profiles $U(z,t)$ converge to the value of U_{10} at $z = 10$ m

$$U_{10} - u_{0L}(t) = \frac{u_*}{\kappa} ln\left(\frac{10-\eta(t)}{z_{oL}(t)}\right) \quad (53)$$

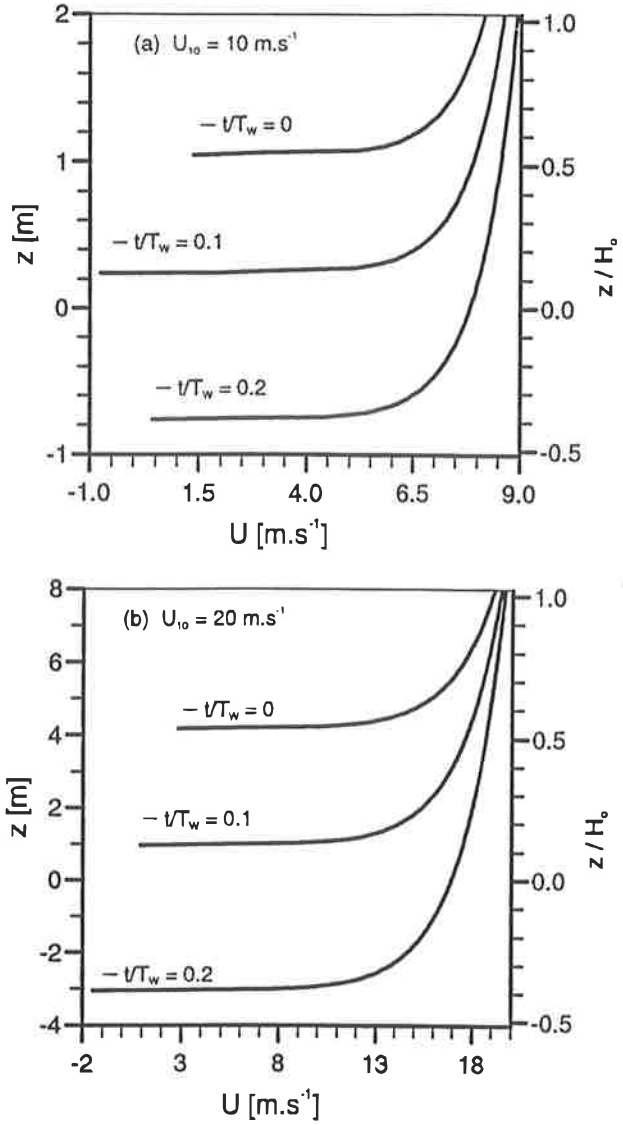

Figure 3. Local wind profiles over the wave for (a) U_{10} = 10 m/s and (b) U_{10} = 20 m/s.

Finally, the average profile $U(z)$ in the wave region is calculated by

$$U(z) = \overline{U(z,t)} = \frac{2}{T_w}\int_0^{T_w/2} U(z,t)\,dt \qquad -H_o/2 < z < H_o \qquad (54)$$

The condition (53) that is imposed to the local profiles is consistent with the simulations of flows over waves that do not present very high steepness and for wind speeds such that H_o < 10 m, about U_{10} < 20 m/s. For simulating flows in very high wind conditions, both the wave profile and this condition will need to be improved.

The number of local profiles must be fairly large (≈500) to obtain a smooth average wind profile in the wave region. Figures 3 and 4 show respectively examples of the local wind profiles $U(z,t)$ for U_{10} = 10 and 20 m/s and the corresponding average wind profile $U(z)$ respectively. A nearly perfect match is observed at the intersection of the upper and wave regions at $z = H_o$. Figure 5 shows $u_{0L}(t)$ and $z_{oL}(t)$. The largest values of u_{0L} and z_{oL} are found at the crest. Note that the mean value of u_{0L} is slightly larger than κu_*, owing to the asymmetry of the Stokes wave. The value of $z_{oL}(t)$ is compared with z_{ou} and with values for the roughness length z_o obtained by Charnock's relation and Kitaigorodskii's model. *Charnock*'s [1955] relation is

$$z_{oc} = a_c \frac{u_*^2}{g} \qquad (55)$$

where g is the acceleration due to gravity and a_c = 0.011 for the open ocean [*Smith*, 1988]. The model of *Kitaigorodskii et al.* [1973] is given by

$$z_{o\kappa} = A_\kappa \left[\int_0^\infty S(\tilde{\omega})\, exp\left(-2\kappa g/\tilde{\omega} u_*\right)\right]^{1/2} \qquad (56)$$

where A_κ = 0.028 [*Geernaert*, 1988] and $S(\tilde{\omega})$ denotes the frequency wave spectrum. $S(\tilde{\omega})$ is taken to be a Philips wave spectrum

$$S(\tilde{\omega}) = \beta\, g^2\, \tilde{\omega}^{-5} \qquad \tilde{\omega} > \omega \qquad (57)$$

where ω is the frequency of the Stokes wave and ß is given by *Geernaert et al.* [1986] for open ocean conditions:

$$\beta = 0.005 + 0.002\,\tilde{\omega} + 1.5\left(\omega u_*/g\right)^2 \qquad (58)$$

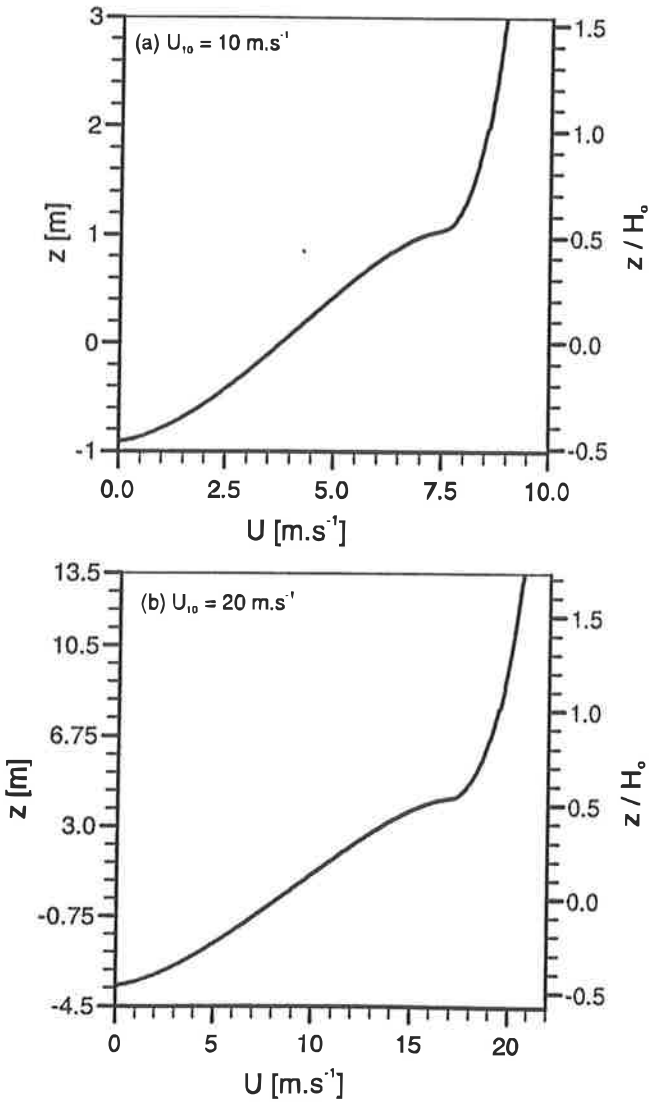

Figure 4. Average wind profile, (a) U_{10} = 10 m/s, (b) U_{10} = 20 m/s.

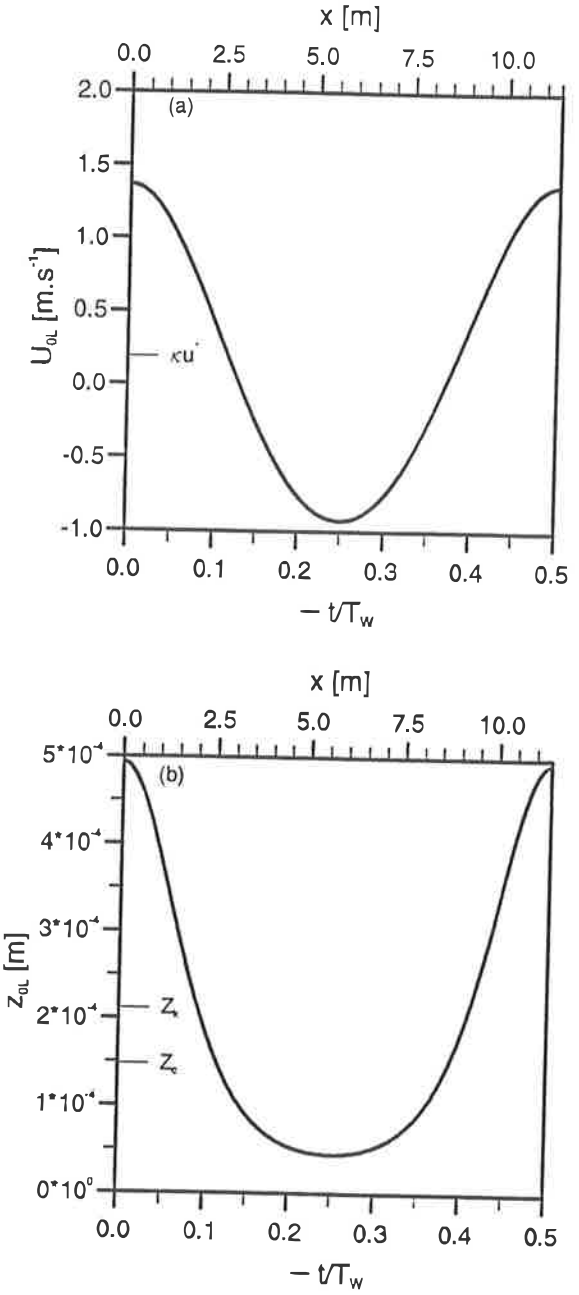

Figure 5. Parameters of the wind profiles (a) Surface value $U(\eta(t),t)$ or $u_{0L}(t)$ as a function of t (b) Local roughness length $z_{0L}(t)$ as a function of t, compared to *Charnock*'s [1955] and *Kitaigorodskii et al*'s [1973] roughness lengths.

Figure 5b shows that the local values z_{oL} are in good agreement with z_{oc} and z_{oK}.

The initial profiles of temperature and water vapor concentration are calculated in almost the same way as the wind profile. In the upper region, where the constant flux assumption is valid in the absence of evaporating droplets, $\nu_t(z)$ is used to calculate $T(z)$ and $\rho_v(z)$:

$$\frac{\partial T}{\partial z} = \frac{T_*}{\kappa z}\varphi_T(z/L)$$
$$\frac{\partial \rho_v}{\partial z} = \frac{\rho_{v*}}{\kappa z}\varphi_v(z/L) \qquad z > H_o \qquad (59)$$

where φ_u/φ_T and φ_u/φ_v are the stability dependent turbulent Prandtl and Schmidt numbers, equal to 1 for $z/L = 0$ (see Section 4). The scaling factors T_* and ρ_{v*} are obtained from the bulk relations (49).

In the wave region the profiles are again computed by averaging in time the local logarithmic profiles $T(z,t)$ and $\rho_v(z,t)$:

$$T(z,t) - T_{ss} = \frac{Pr_T T_*}{\kappa} ln\left(\frac{z-\eta(t)}{z_{oTL}(t)}\right)$$
$$\rho_v(z,t) - \rho_{vss} = \frac{Sc_T \rho_{v*}}{\kappa} ln\left(\frac{z-\eta(t)}{z_{ovL}(t)}\right) \qquad \eta(t) \le z < H_o \qquad (60)$$

where we assume that the surface temperature and water vapor concentration do not vary along the wave. The local temperature and humidity roughness length $z_{oTL}(t)$ and $z_{ovL}(t)$ do depend on t and are again found by imposing the condition that all local profiles converge to T_{10} and ρ_{v10}, respectively, at z = 10 m:

$$T_{10} - T_{ss} = \frac{Pr_T T_*}{\kappa} ln\left(\frac{10-\eta(t)+z_{oTL}(t)}{z_{oTL}(t)}\right)$$
$$\rho_{v10} - \rho_{vss} = \frac{Sc_T \rho_{v*}}{\kappa} ln\left(\frac{10-\eta(t)+z_{ovL}(t)}{z_{ovL}(t)}\right) \qquad (61)$$

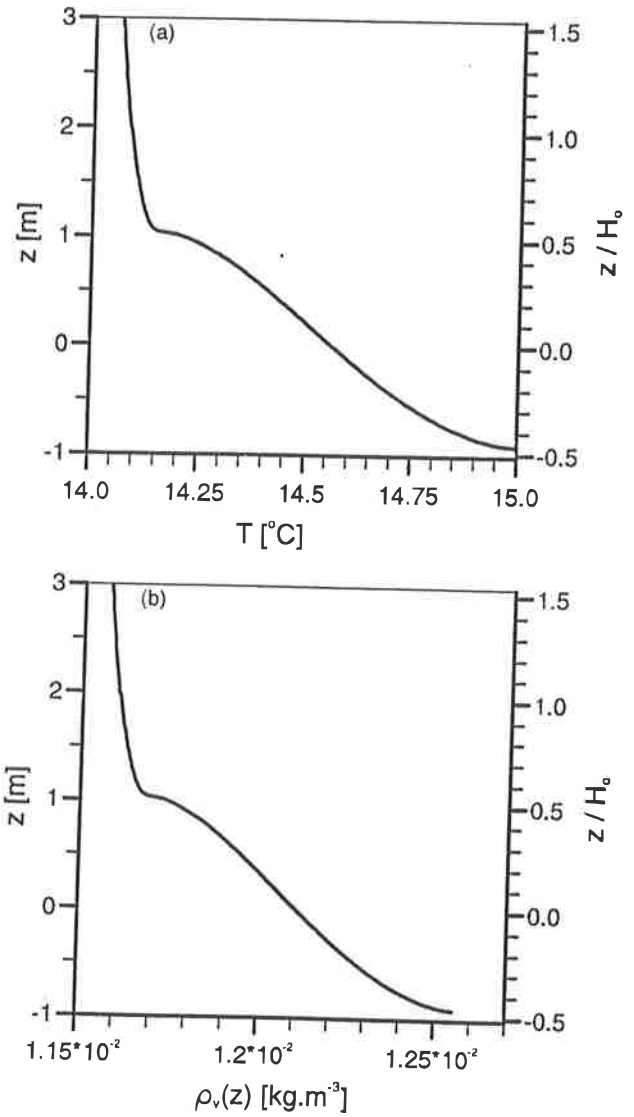

Figure 6. Average profiles of (a) temperature and (b) water vapor concentration (U_{10} = 10 m/s, T_{10} = 14°C, RH_{10} = 95%, T_{surf} = 15°C).

with $\rho_{v10} = RH_{10}\cdot\rho_{v\,sat}(T_{10})$. The average profiles $T(z)$ and $\rho_v(z)$ in the wave region are calculated by integrating the local profiles over the wave surface. Just as in the case of the wind profile, the number of local profiles should be about 500. Figure 6 shows examples of these averaged profiles for T_{10} = 14°C, RH_{10} = 95%, and T_{surf} = 15°C (and U_{10} = 10 m/s). Note that the profiles of the upper region and of the wave region match perfectly at the intersection ($z = H_o$).

The vertical component of the local mean wind speed is obtained from the horizontal wind speed component using the continuity equation for a steady, homogeneous flow [e.g., *White*, 1988]:

$$\frac{\partial U}{\partial x} = -\frac{\partial W}{\partial z} \tag{62}$$

where $x = -C_w t$ and U is obtained from the individual local profiles $U(z,t)$; see (51). The resulting wind field $W(z,t)$ also consists of local profiles, constructed by steps from the values of W at the wave surface. $W(\eta(t),t)$ is equal to the local vertical velocity of the wave surface:

$$W(\eta(t),t) = W_s(t) = \frac{\partial \eta}{\partial t} \tag{63}$$

The computation of the continuity equation presents some numerical difficulties which are mainly due to the strong gradients of U and W in the immediate vicinity of the surface. This requires an especially adapted computation grid, constant at all altitudes except close to the surface with very narrow spacings (for numerical implementation procedures see *Van Eijk et al.* [1993]). Although (54) uses only the local profiles up to H_o, the values of $U(z,t)$ and $W(z,t)$ are normally computed up to the altitudes required by the computation of droplet trajectories (see section 3.3), while the full 2-D flow field can also be computed up to z = 10 m to verify the precision of the calculation.

Figure 7 shows results for a calculation of $W(z,t)$ in the case U_{10} = 10 m/s, where 1000 local U profiles were used. The wave travels to the right and the z grid has Nz grid points between $z = -H_o/2$ and z = 10 m. Figures 7a and 7b show the surface vertical velocity as a function of t and the local wind profiles $W(z,t)$ at various locations over the wave, respectively, obtained with Nz=10,000. The success of the calculation of the local profiles $W(z,t)$ may be verified in the region well above the waves, where the waves no longer have any influence on the velocity field. Thus, in that region, $W(z,t)$ should be close to zero. Figure 7c shows $W(z,t)$ at a height of 10 m ($\approx 5.1H_o$ for U_{10}=10 m/s) as a function of t. It was constructed by taking the value $W(z=10,t)$ of each of the local profiles $W(z,t)$. The curve marked by plus signs was obtained from local profiles $W(z,t)$ that had been calculated with 1000 vertical grid points between the surface and 10 m AMSL, the curve marked by crosses from local profiles $W(z,t)$ that had 10,000 vertical grid points. It is easily seen from Figure 7c that Nz should be of the order of 10^4 to obtain a wind field $W(z,t)$ that is independent of t and close to zero above the wave region.

Since both $U(z,t)$ and $W(z,t)$ are now determined, a vector plot of the wind field over the wave can be constructed. Such plots are shown in Figure 8 for U_{10} = 10 and 20 m/s, where the length and direction of the arrows represent wind speed and wind direction, respectively, relative to the surface, i.e. vectors of components $(U-C_w, W)$. The model that describes the effect of the surface motion on the air flow results in a perfectly symmetric wind field with a rotor-like structure between the wave crests. The influence of the waves decreases with height and becomes negligible above 2-3H_o. *De Leeuw* [1987] hypothesized that the rotor structure is responsible for the nonlogarithmic droplet concentration profiles. This structure is also observed in *Edson*'s [1990] simulations of flows over developed waves, with a flow model

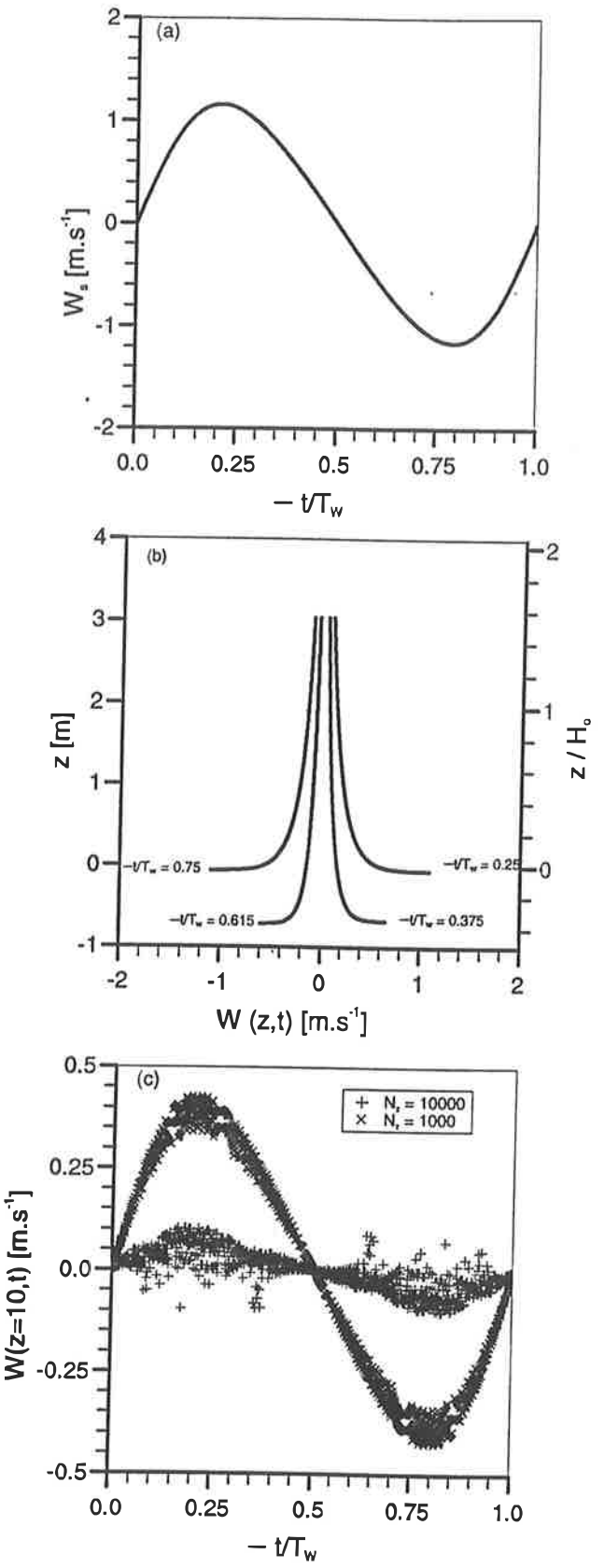

Figure 7. Parameters for the mean flow field over the waves: (a) wave surface vertical velocity, (b) local profiles of the vertical wind component, and (c) vertical wind component distribution at z = 10 m (see text).

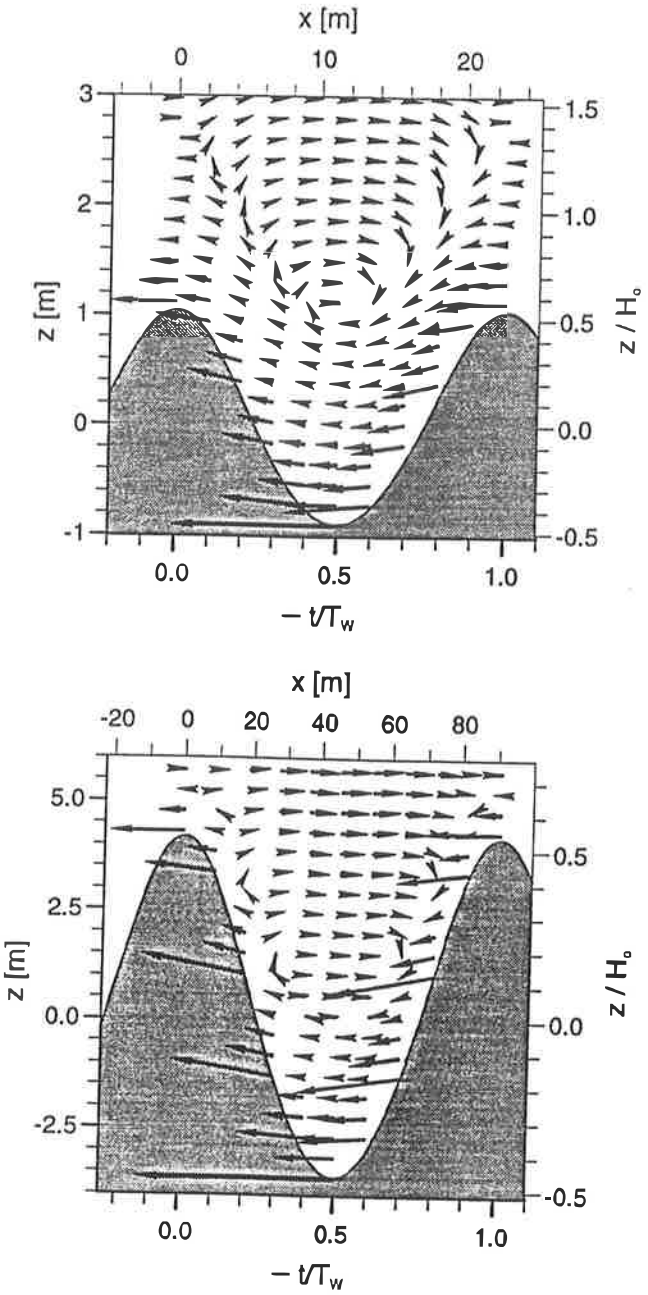

Figure 8. Mean wind field over the waves for (a) U_{10} = 10 m/s and (b) U_{10} = 20 m/s.

that is mathematically different but physically close to the model described here. Note in Figure 8 the difference in the rotor location at 10 and 20 m/s. While at 20 m/s its center is close to $z = 0$ and it extends to about $z = H_o$, at 10 m/s its center is slightly higher than the wave crest and it extends higher than $z = 2H_o$. Of course, the structure of the flow depends on the assumptions of the model. In particular, the symmetry of the flow is linked to the symmetry of the wave profile. The sensitivity of the results to the model assumptions is still under study, but the simulations already done show that the general features of the mean flow do not change with the values of the basic parameters h and Γ.

In the discussion following *Edson*'s [1990] presentation [see *Mestayer et al.*, 1990a] it was proposed that, if this rotor structure dominates the turbulent field in the lowest part of the marine atmospheric surface layer, its effect can be modeled in the eddy diffusivity by considering that between trough and crest the turbulence mixing length is not proportional to z but constant with height and equal to the wave height, i.e.,

$$\begin{aligned} \nu_t(z) &= \kappa u_* z/\varphi_u(z/L) && z \geq +H_o/2 \\ \nu_t(z) &= \kappa u_* (H_o/2)(t_+(z)/T_w) && z \leq +H_o/2 \end{aligned} \qquad (43')$$

where $t_+(z)/T_w$ is the fraction of time when the height z is above the wave surface. The eddy diffusivity profiles obtained with these relationships are shown in Figure 2 for comparison (dashed lines). Yet in SeaCluse, where the mean motion of the droplets and their dispersion by turbulence are modeled separately, it is preferred to consider that the rotor-like flow structure belongs to the mean motion and that the turbulent diffusivity scales with height as in all flows where the turbulent field is generated by surface stress.

3.3 Droplet Mean Motion Over the Waves

To calculate the trajectories of sea spray droplets that are generated by bursting bubbles, the first parameter that is required is the ejection velocity $V_e(r)$. In the present version of SeaCluse, only jet droplets are considered, as a consequence of the lack of knowledge on the initial dynamics of the spume droplets. The ejection heights $H_e(r)$ of the droplets are inferred from Blanchard's ejection data [*Blanchard*, 1963, 1989]. The ejection velocities $V_e(r)$ are computed from $H_e(r)$ by an iterative procedure described previously [*Wu*, 1979; *Rouault et al.*, 1991]. The method uses the equation of vertical motion in nonturbulent and nonevaporative conditions over a horizontal still surface and an initial guess for $V_e(r)$ to infer the maximum height $H(r)$ that the droplet reaches; the value for $V_e(r)$ is then gradually adjusted until $H(r) = H_e(r)$. Actually, as noted by an unknown reviewer, Blanchard's data were obtained in evaporative conditions, usually 80% RH, while these calculations assume no evaporation. Yet the changes in the ascending part of the droplet trajectories are very small, and the resulting errors on the initial velocities are negligible. Nevertheless, this will be taken into account in the near future when recomputing these data from the newer measurements of *Spiel* [1992, 1994].

The presence of waves complicates the calculation of the droplet trajectories because the horizontal displacement of the droplet and the motion of the air itself must also be taken into account. The trajectories are most conveniently calculated in the coordinate system that moves along with the waves with celerity C_w. In this system, at time t' the droplet has a position given by its coordinates x_d, z_d that are a function of the air flow and of the position x_e where it was ejected from the wave surface. The horizontal and vertical components of the droplet velocity u_d and w_d are given by

$$\begin{aligned} u_d(r, x_e, t') &= u_r(r, t') + U(x_d, z_d) - C_w \\ w_d(r, x_e, t') &= w_r(r, t') + W(x_d, z_d) \end{aligned} \qquad (64)$$

where $U(x_d,z_d)$ and $W(x_d,z_d)$ are the local horizontal and vertical air velocity components and $u_r(r, t')$ and $w_r(r, t')$ denote the horizontal and vertical velocity of the droplet relative to the air. At each position of the droplet, $U(x_d,z_d)$ and $W(x_d,z_d)$ are computed by a four-point interpolation from the four closest tabulated values of the local wind speed profiles $U(z,t)$ and $W(z,t)$, with $z = z_d$ and $t = -x_d/C_w$. The equations of droplet motion are

$$\frac{\partial u_r}{\partial t'} = -\frac{3}{8} C_D \frac{\rho_a}{\rho_w} \frac{u_r |u_r|}{r}$$
$$\frac{\partial w_r}{\partial t'} = -\frac{3}{8} C_D \frac{\rho_a}{\rho_w} \frac{w_r |w_r|}{r} - g \quad (65)$$

where C_D denotes the air drag coefficient. For a spherical droplet, C_D is a function of the Reynolds number Re_d

$$Re_d = \frac{2r\left(u_r^2 + w_r^2\right)^{1/2}}{\nu} \quad (66)$$

and it is calculated with *Raudviki*'s [1979] formula:

$$\begin{aligned} C_D &= 24/Re_d & Re_d &< 0.5 \\ C_D &= 24\left(1+0.19\,Re_d\right)/Re_d & 0.5 \le Re_d &< 2 \\ C_D &= 24\left(1+0.15\,Re_d^{0.687}\right)/Re_d & 2 \le Re_d & \end{aligned} \quad (67)$$

The droplet initial relative velocities $u_r(r, t' = 0)$ and $w_r(r, t' = 0)$ are given by:

$$\begin{aligned} u_r(r, t'=0) &= 0 & u_d(r, x_e, t'=0) &= u_{0L}(x_e) - C_w \\ w_r(r, t'=0) &= V_e(r) & w_d(r, x_e, t') &= V_e(r) + W_s(x_e) \end{aligned} \quad (68)$$

where $W_s(x_e)$ is the surface vertical velocity $W_s(t = x_e/C_w)$.

The droplet trajectory is computed with (64)-(68) and stopped when the droplet hits the water surface, i.e., when $z_d \le \eta(x_d)$. To improve the precision, the calculation is done in a grid that is equidistantly spaced along the droplet trajectory, with constant steps $\Delta l(r)$, i.e., by recalculating $\Delta t'$ in each cycle:

$$\Delta t'(r, t') = \Delta l(r) \cdot \left[u_d\left(r, x_d, z_d, t'\right)^2 + w_d\left(r, x_d, z_d, t'\right)^2 \right]^{-1/2} \quad (69)$$

The time step $\Delta t'$ is small when the droplet velocity with respect to the wave surface is large (this means that the relative velocity (u_r, w_r) of the droplet is large, and/or the droplet is at a position (x_d, z_d) where the wind field (U, W) is strong) whereas it becomes larger when the droplet slows down. The step size $\Delta l(r)$ depends on the size of the droplet and varies between 0.02 and 0.5 cm for $10 \le r \le 250$ μm.

Examples of typical trajectories are shown in Figure 9 (U_{10} = 10 m/s) for different diameters and different places of ejection (since the droplets travel more slowly than the wave, all trajectories here are from right to left in the wave-following coordinate system). Different trajectories are obtained when droplets are ejected from the lee side of the wave. They do not simply fall back, but are lifted upward and enter in the wave rotor (Figures 9b and 9c). In some cases, they return to the surface (Figure 9b), but in other cases they start to move in a closed trajectory (Figure 9c). Clearly, the criterion that the trajectory calculation is finished when the droplet hits the surface again does not work for droplets moving in a closed trajectory. These closed trajectories are thought to be an artefact resulting from the perfect symmetry of the air flow model. In reality, the wave surface is not perfectly smooth, and small variations in $\eta(x)$ induce asymmetry in the wave rotor, with the consequence that the droplets do not move indefinitely in a perfectly closed loop. Therefore the alternative

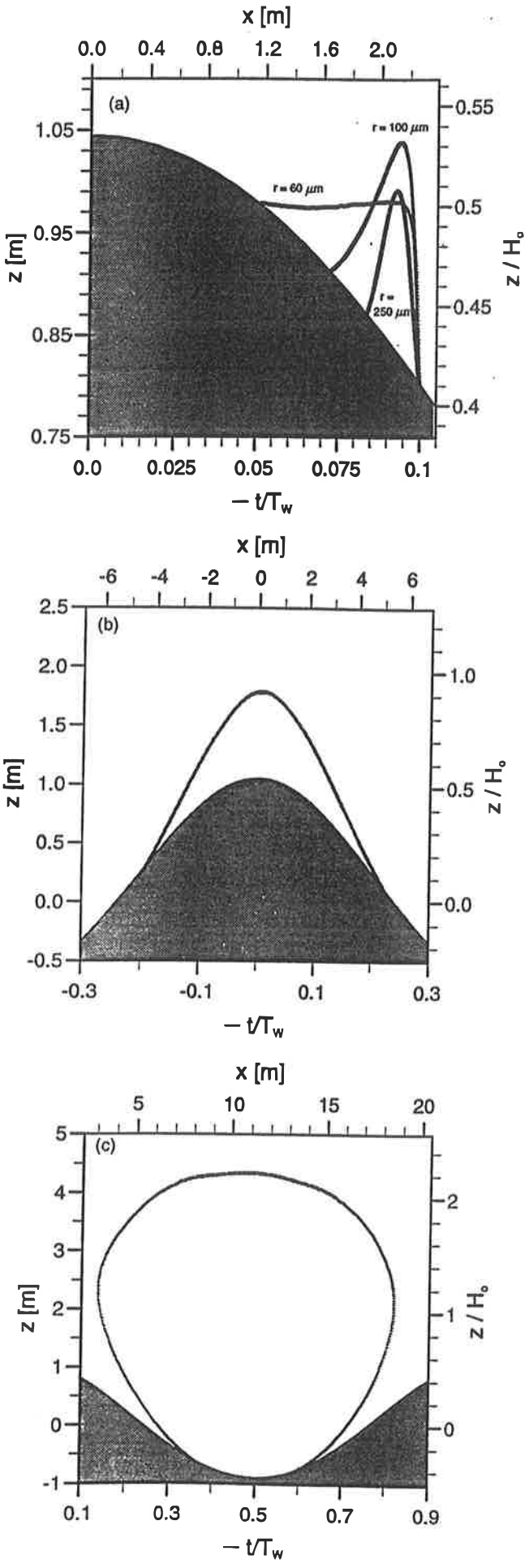

Figure 9. Representative droplet trajectories (U_{10} = 10 m/s) (a, b) Trajectories not influenced by the wave rotor (c) Trajectory entering the wave rotor.

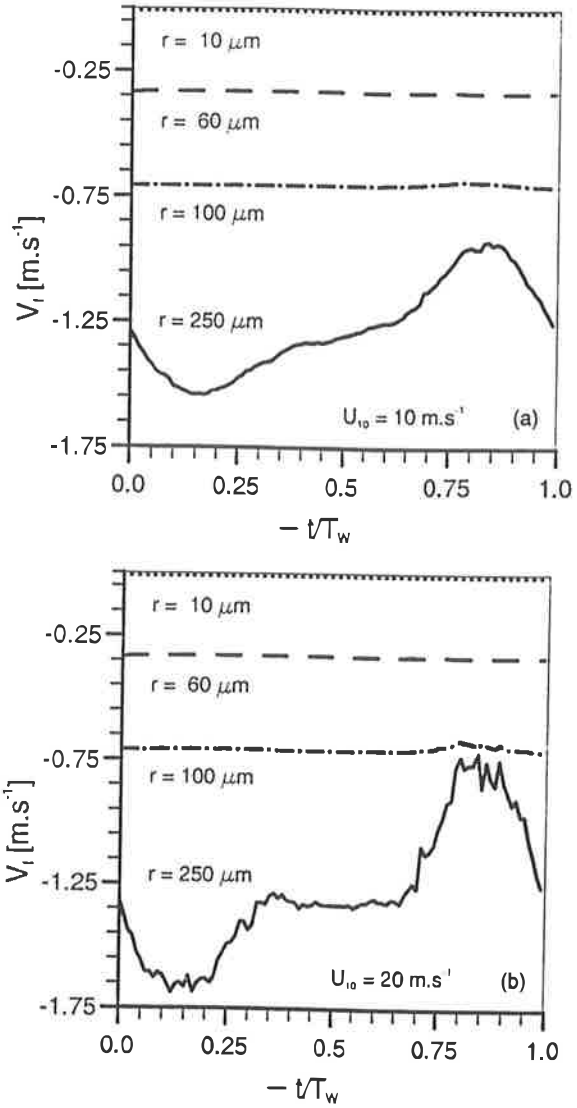

Figure 10. Final fall velocities V_f over the wave as a function of ejection time t, for droplets with radii of 10, 60, 100, 250 μm for (a) U_{10} = 10 m/s and (b) U_{10} = 20 m/s.

criteria for ending the trajectory calculation are actually the following: when the droplet has passed $x = x_e$ for a second time and starts to move away from the wave surface, or when $z_d \leq \eta(x_d) + \Delta\eta/2$, where $\Delta\eta = \max(z_{oL}(x_e), 3\text{ mm})$ accounts for the presence of capillary waves at the surface of the Stokes wave.

The computation of series of droplet trajectories, for all positions x_e of the source and for all diameters, makes it possible to obtain the parameters necessary for SeaCluse calculations: final fall velocities, flight times, and normalized reference concentration profiles.

The final fall velocity for each droplet is its vertical velocity component at the last time step of its trajectory. Figures 10 and 11 display these values as a function of the droplet initial position, expressed in terms of the ejection time with respect to the wave period. Figure 10 compares the variations of V_f for four typical categories of droplets, 10-, 60-, 100- and 250-μm radius, for U_{10} = 10 m/s (Figure 10a) and 20 m/s (Figure 10b): only the larger droplets experience large variations of V_f; the larger fall velocities being found at the lee side of the wave, where the trajectories are longer, as shown below. The final fall velocity of the 10-μm droplets is independent of the start of the trajectory, since they all rapidly reach their limit velocity. Figure 11 details the comparison of V_f for the two wind speeds, for each of the three larger categories. The figure shows that V_f does not vary much with wind speed, although it must be noted that the Stokes wave amplitude $H_0/2$ is 4 times larger at 20 m/s than at 10 m/s.

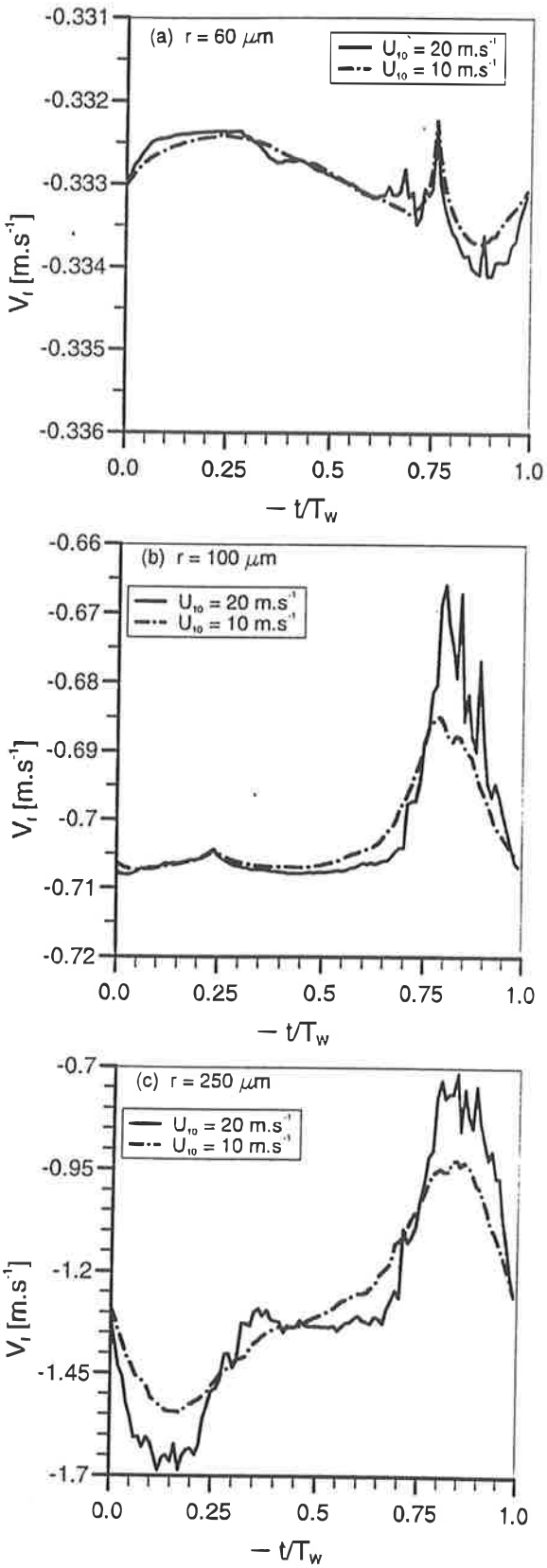

Figure 11. Comparison of final fall velocities V_f over the wave as a function of ejection time t, for U_{10} = 10 m/s and U_{10} = 20 m/s: (a) r = 60 μm, (b) r = 100 μm, and (c) r = 250 μm.

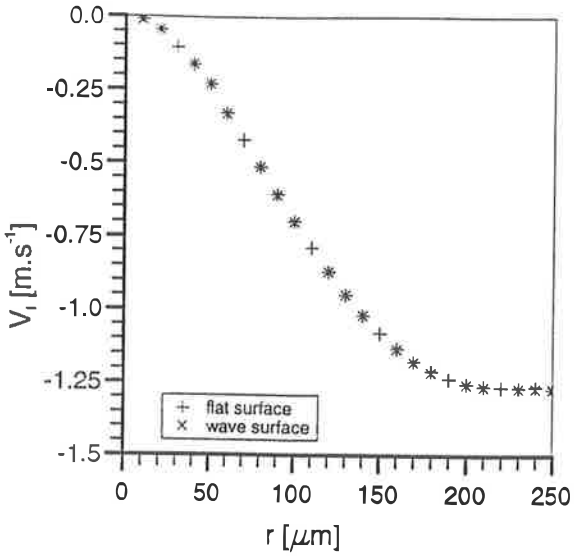

Figure 12. Average final fall velocities for droplets over the waves (plus signs) and over a flat surface (crosses).

Figure 12 shows the average final fall velocities $V_f(r)$ versus r after integration along the wave surface, compared to the final fall velocities over a flat surface: the two curves are nearly identical. For the sake of comparison, the terminal free fall velocities V_g of these droplets are 0.012, 0.332, 0.704, and 2.02 m/s, respectively. Figure 3 of *Rouault et al.* [1991] showed that, over a flat surface $V_f = V_g$ for all droplets with $r < 120$ μm.

The flight time $T_{fly}(r,x_e)$ or suspension time of the droplet is the total duration of the trajectory. Figure 13 presents plots of T_{fly} as a function of droplet ejection time for the four typical size categories, for U_{10} = 10 and 20 m/s. The flight time is larger when the droplets are ejected from the lee side of the wave where the surface moves up and propels them into air that itself is moving upward. The opposite effect is observed at the windward side of the wave, where the air moves down and shortens the flight time. This different behavior is especially striking for the smallest droplets with 10-μm radius, which have extremely short suspension times on the windward side where they are "aspirated back" to the surface, and extremely long flight times on the lee side where they are entrained in the "rotor" and experience

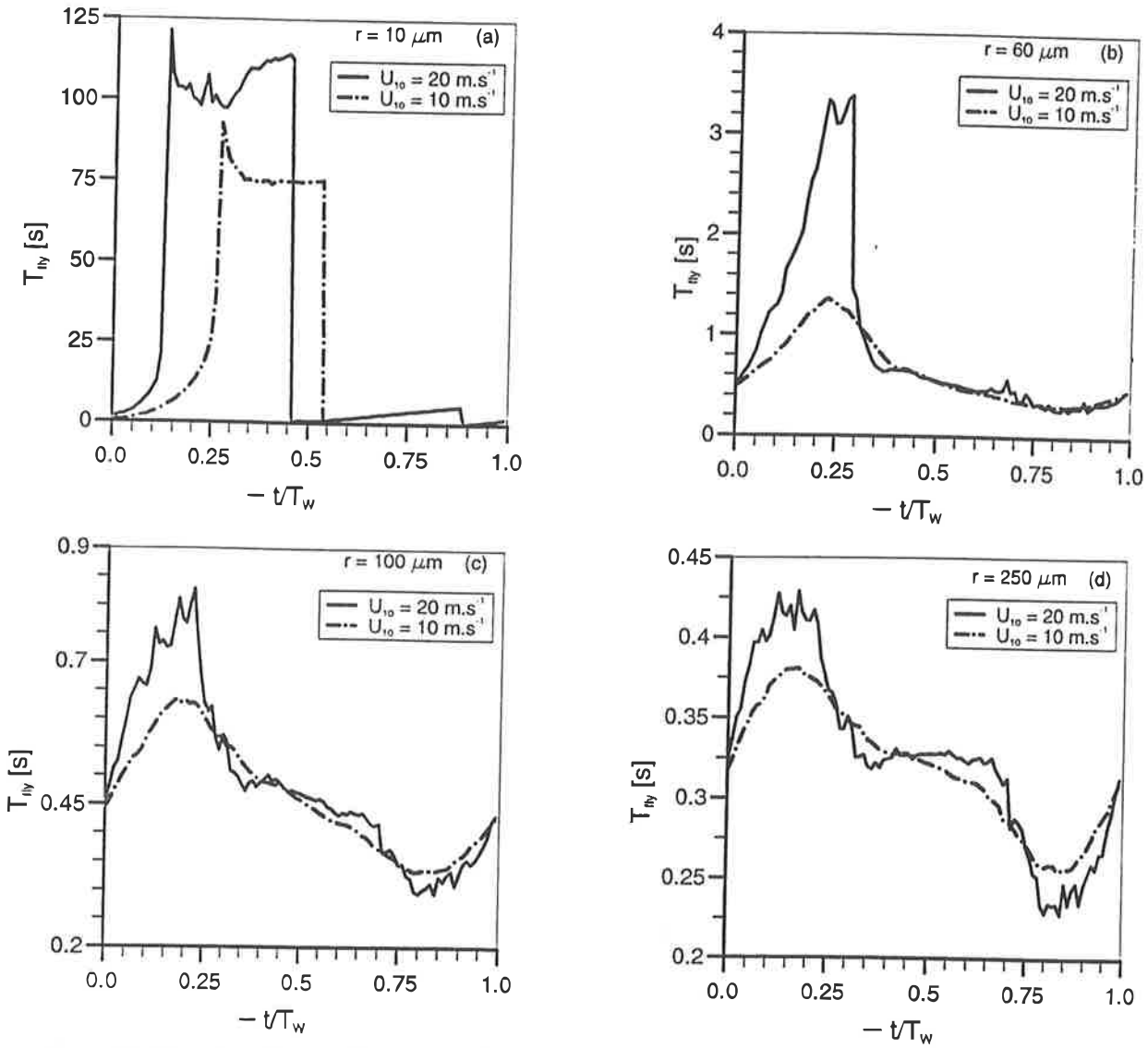

Figure 13. Flight times T_{fly} over the wave as a function of ejection time t, for U_{10} = 10 m/s and U_{10} = 20 m/s: (a) r = 10 μm, (b) r = 60 μm, (c) r = 100 μm, and (d) r = 250 μm.

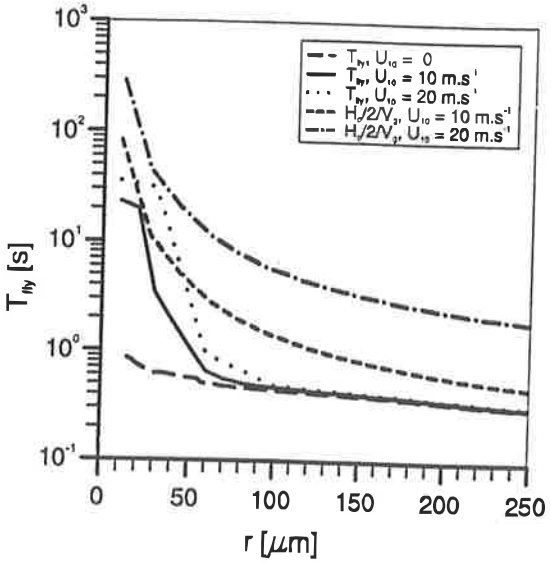

Figure 14. Average flight times as a function of droplet radius, for droplets over the wave (U_{10} = 10 and 20 m/s) and over a flat surface (U_{10} = 0), compared to *Andreas*' [1992] suspension times $A_{1/3}/V_g(r)$ (U_{10} = 10 and 20 m/s).

closed loop or spiralling trajectories (see Figure 9c). Larger droplets experience lengthened trajectories of the type illustrated in Figure 9b. The flight time dependence on wind speed U_{10} is extremely small, except around the maximum on the lee side of the wave. While its amplitude does not vary with U_{10}, the position of this maximum shifts toward the wave crest with increasing radius, while the maximum of the surface vertical velocity $\partial\eta/\partial t$ takes place at $-t/T_w = 0.25$.

The average flight times obtained by integrating over the wave period

$$T_{\mathrm{fly}}(r) = \frac{1}{T_w}\int_{t=0}^{T_w} T_{\mathrm{fly}}(r,t)\,dt \qquad (70)$$

are the parameters entered in SeaCluse equations (18) and (21), $T_{\mathrm{fly},n} = T_{\mathrm{fly}}(r_n)$, when a homogeneous distribution of droplet sources is considered. The values of $T_{\mathrm{fly}}(r)$ are shown in Figure 14 as a function of r, for the two wind speeds 10 and 20 m/s. Three other curves are also included in this figure for comparison: the flight times over a flat surface (identical to $U_{10} = 0$) and the residence times of *Andreas* [1992] as given in (13), i.e., the time for the droplets to fall from the wave crest to mean sea level at its free-fall limit velocity, $^1/_2 H_o/V_g$. This figure shows that, for all droplets larger than ~ 90-μm radius, the average flight times are not significantly influenced by the waves and the wind velocity, while Andreas' residence times increase about as U_{10}^2, as shown by (40)-(42). This results in timescales larger than those obtained here by about a factor 2-4 at 10 m/s and a factor 6-12 at 20 m/s. Figure 15 portrays the maximum flight times obtained from the wave lee side for each droplet radius, compared to the same three curves. These maximum flight times could be representative of the behavior of the spume droplets (note, however, that they do not correspond to droplets ejected from the wave crest). The figure shows that the maximum flight times increase a little with wind speed, by about a constant factor of 25% from 10 to 20 m/s, but are still 4 times smaller than Andreas' residence times. Actually, (40)-(42) with $h = 0.135$ and $\Gamma = 0.85$ yield $H_o/2 \approx 0.01\ U_{10}^2$, while *Andreas* [1992] used $A_{1/3} = 0.015\ U_{10}^2$, which gives even larger values by about 50%. Nevertheless, these new results do not take into account the effect of diffusion by turbulence, and it is important to quantify this effect for the different droplet sizes before drawing conclusions: this will be done in sections 4 and 5, respectively.

3.4 Reference Profiles of Droplet Concentrations

The reference profiles $\rho_n^o(z)$ used to model the mean momentum terms in droplet equation (18) correspond to conditions with no turbulent diffusion and no evaporation, while the wind field in which the droplet trajectories are computed is the mean turbulent wind field. This method separates the effects of turbulence on the air flow and on the droplet dispersion.

The profiles $\rho_n^o(z)$ are constructed by recording the residence times of the droplets in each grid mesh during their trajectories described above. If $T_{r,t}(z-\Delta z/2, z+\Delta z/2)$ is the time of residence of the droplet, ejected at a position t from the wave surface, within the grid mesh centered on height z, then

$$p_{r,t}(z-\Delta z/2, z+\Delta z/2) = T_{r,t}(z-\Delta z/2, z+\Delta z/2)/T_{\mathrm{fly}}(r,t) \qquad (71)$$

is the probability of finding this droplet in the height interval $[z-\Delta z/2, z+\Delta z/2]$, i.e., the (fractional) number of droplets of radius r observed in this z interval if one droplet is ejected from the surface every $T_{\mathrm{fly}}(r,t)$ time interval. If one droplet is ejected per second, the observed number of droplets is $p_{r,t}\,T_{\mathrm{fly}}(r,t) = T_{r,t}$. If the surface flux of droplets is 1 droplet per m^2 per second, then $T_{r,t}(z-\Delta z/2, z+\Delta z/2)\,/\,\Delta z$ is the concentration of droplets of radius r observed per unit volume in grid mesh z (in droplets per m^3). The t dependency is removed by taking the sum of the contributions of the M computed individual droplets ejected at various positions t over the wave surface:

$$\xi_r(z-\Delta z/2, z+\Delta z/2) = \frac{1}{\Delta z}\frac{1}{M}\sum_{m=1}^{M} T_{r,t_m}(z-\Delta z/2, z+\Delta z/2)$$
$$\xi_r(z) = \lim_{\Delta z \to 0} \xi_r(z-\Delta z/2, z+\Delta z/2) \qquad (72)$$

Here, $\xi_r(z)$ is the droplet concentration normalized by the surface flux, in (droplets/m^3) / (drop/m^2/s) or s/m. It appears as a "transfer function" of the droplet dynamics, from the surface

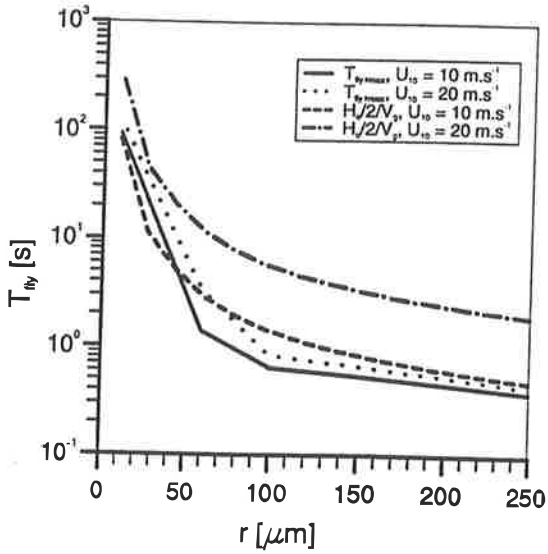

Figure 15. Same as Figure 14, except that the maximum flight times over the wave are shown (U_{10} = 10 and 20 m/s).

source function to the concentration in air. Thus

$$\left(\frac{dN}{dr}\right)^{o} = \xi_r(z)\cdot\left(\frac{dF}{dr}\right) \tag{73}$$

and

$$\rho_n^o(z) = \left(\frac{dN}{dr}\right)_{r_n}^{o}\left(\frac{4}{3}\pi\, r_n^3\,\rho_w\right)\Delta r_n = \xi_{r_n}(z)\left(\frac{dF}{dr}\right)_{r_n}\left(\frac{4}{3}\pi r_n^3\rho_w\right)\Delta r_n = \xi_{r_n}(z)\,\rho_n^e\,w_n^e \tag{74}$$

where $\rho_n^e w_n^e$ is defined by (27), and where the superscript o denotes the absence of turbulence and evaporation. The number of individual droplet trajectories needed to obtain a representative transfer function depends on the wind speed U_{10}, which determines the wave height; it must be higher than 200 for the largest wind speeds for which the SeaCluse model is developed (U_{10} = 25 m/s).

The reference transfer functions $\xi_{r_n}(z)$ computed by the preprocessor for a given value of U_{10} (and a given set of wave parameters h and Γ) are stored for further use by the main program SeaCluse. In the latter the reference profiles $\rho_n^o(z)$ can be computed using (74) with a given empirical surface source function to simulate a given situation, i.e., the source function dF/dr is prescribed in the model. Alternatively the ρ_n^e values can be adjusted in (30) and (74) to match the simulation results to experimental data to deduce the actual surface source function from (27). In order to be independent of the choice of the source function, the results of the present simulations are normalized by the surface fluxes, i.e., the reference (nonturbulent) transfer functions $\xi_{r_n}(z)$ are compared, in the next section, to the normalized concentrations $\rho_n(z)/(\rho_n^e w_n^e)$ obtained with the main program including turbulent diffusion.

4. Droplet Dispersion By Turbulence

In the equations for vapor concentration (17c) and heat (17d), the turbulent flux terms 3 are modeled by introducing the classical exchange coefficients:

$$\overline{\rho_v' w'} = -K_v\frac{\partial\overline{\rho_v}}{\partial z} = -\frac{\nu_t}{Sc_T}\frac{\partial\overline{\rho_v}}{\partial z} \tag{75a}$$

$$\overline{T'w'} = -K_T\frac{\partial\overline{T}}{\partial z} = -\frac{\nu_t}{Pr_T}\frac{\partial\overline{T}}{\partial z} \tag{75b}$$

where Sc_T and Pr_T are the turbulence Schmidt and Prandtl numbers and ν_t is the eddy viscosity function calculated by the preprocessor (see Section 3). In neutral conditions, following the reevaluation of *Högström* [1988],

$$Sc_T = Pr_T = 1 \tag{76}$$

while the original CLUSE model used a value of 0.74 for laboratory flows.

To take into account the effect of droplet inertia in the turbulent diffusion, *Rouault et al.* [1991] introduced the phase slip velocity $\Delta_{\gamma j}$ relative to the fluid

$$V_{\gamma j} = V_j + \Delta_{\gamma j} \tag{77}$$

where, because of the basic hypothesis 7, only the particulate phase (i.e. the droplets) have a nonzero slip velocity: $V_{aj} = V_{vj} = V_j$. Thus the droplet vertical velocity is written

$$W_n = \overline{W}_n + w_n' = \overline{W}_n + w_a' + \Delta_{nz}' \tag{78}$$

with $\overline{W}_n = \overline{\Delta_{nz}}$, since $\overline{W} = \overline{W}_a = 0$. Using (78), it is possible to rewrite term 3 of (17b) as

$$\frac{\partial\left(\overline{\rho_n' w_n'}\right)}{\partial z} = \frac{\partial\left(\overline{\rho_n' w_a'}\right)}{\partial z} + \frac{\partial\left(\overline{\rho_n'\Delta_{nz}'}\right)}{\partial z} \tag{79}$$

3 3′ 3″

Term 3′ is similar to terms 3 of (17c) and (17d). It represents the diffusion by air turbulence and is modeled by means of an exchange coefficient equal to that of vapor:

$$\overline{\rho_n' w_a'} = -K_n\frac{\partial\overline{\rho_n}}{\partial z} = -\frac{\nu_t}{Sc_T}\frac{\partial\overline{\rho_n}}{\partial z} \tag{80}$$

and term 3″ represents the effect of droplet inertia on the turbulent motion, i.e., a reduction of turbulence diffusion. *Rouault et al.* [1991] modeled this "counter-diffusion" term with a size-dependent exchange coefficient:

$$\overline{\rho_n'\Delta_{nz}'} = -K_n'\frac{\partial\overline{\rho_n}}{\partial z},\quad K_n' = -\frac{\nu_t}{Sc_n}\left[1-\left(1+C_2\frac{V_f^2(r_n)}{\sigma_w^2}\right)^{-1}\right] \tag{81}$$

where the air vertical velocity variance was modeled by the atmospheric surface layer relation

$$\sigma_w = 1.25u_* \tag{82}$$

[e.g., *Panofsky and Dutton*, 1984] which is also verified in the IMST wind-wave tunnel [e.g., *Edson and Fairall*, 1994], and a value of 5 was obtained for the constant C_2 by adjustment to the experimental data obtained during the HEXIST-CLUSE experiment. Therefore, in the atmospheric surface layer where σ_w = $1.3u_*$, the model of *Rouault et al.* [1991] (RMS) becomes

$$\overline{\rho_n' w_n'} = \overline{\rho_n' w_a'} + \overline{\rho_n'\Delta_{nz}'} = -\left(K_n + K_n'\right)\frac{\partial\overline{\rho_n}}{\partial z}$$
$$K_{n\mathrm{RMS}} = K_n + K_n' = \frac{\nu_t}{Sc_T}\left[1+C_2\frac{V_f^2(r_n)}{1.56\,u_*^2}\right]^{-1}\quad C_2 = 5 \tag{83}$$

Alternatively, other authors proposed to directly model the particle flux term $\overline{\rho_n' w_n'}$ with an exchange coefficient based on a variable Schmidt number, depending on particle inertial scales

$$\overline{\rho_n' w_n'} = -\frac{\nu_t}{Sc_n}\frac{\partial\overline{\rho_n}}{\partial z},\quad Sc_n = Sc_n(u_*, r_n, \ldots) \tag{84}$$

Two models are analyzed here: the first one (called MM) is derived from the work of *Mostafa and Elgobashi* [1984] and *Mostafa and Mongia* [1987], and the second one (called MB) from *Melville and Bray* [1979]. Both original models were derived from the pioneering analysis of *Meek and Jones* [1973] to simulate two-phase turbulent jets. The original MM model is expressed by

$$Sc_n = \left(1+0.3\,\frac{\left|\mathbf{V}-\mathbf{V}_n\right|^2}{\left[\overline{v}_n\right]^2}\right)^{1/2} \tag{85}$$

where the rms of the droplet velocity is given by

$$\frac{\left[\overline{v}_n\right]^2}{\overline{u'^2}} = \frac{1}{1+\tau_n/\tau_L} \tag{86}$$

where τ_L is the Lagrangian timescale of the flow and τ_n the timescale for the droplet inertial drag, given by

$$\tau_n = \frac{8 r_n \rho_w/\rho_a}{3 C_D \left|\mathbf{V}-\mathbf{V_n}\right|} \tag{87}$$

The constant 0.3 in (85) was optimized by comparison to previous experimental data. For application to the marine atmospheric surface layer, SeaCluse models τ_L by

$$\tau_L = \nu_t(z)/\sigma_w^2 = \nu_t(z)/\left(1.56 u_*^2\right) \tag{88}$$

$\overline{u'^2}$ by $\sigma_u^2 = \left(2.39 u_*\right)^2$ [*Panofsky and Dutton*, 1984]), and the slip velocity modulus $\left|\mathbf{V}-\mathbf{V_n}\right|$ by the gravitational free-fall velocity $V_g(r_n)$ in (85) and (87); C_D is obtained from (66)-(67) with $Re_d = 2 r_n V_g(r_n)/\nu$. The MM model then becomes

$$K_{n\mathrm{MM}} = \frac{\nu_t}{Sc_T}\left[1+0.3\frac{V_g^2(r_n)}{5.71 u_*^2}\left(1+\frac{1.56 u_*^2\, 8 r_n \rho_w/\rho_a}{3\, C_D\, V_g(r_n)\, \nu_t(z)}\right)\right]^{-1/2} \tag{89}$$

where Sc_T has been added for consistency with gas diffusivity when $r_n \to 0$.

The MB original model can be written as

$$K_n/K_T = \overline{V_n'^2}/\overline{V'^2} = \left(1+\tau_{*n}/\tau_L\right)^{-1} \tag{90}$$

where τ_{*n} is the Stokes relaxation timescale, the response time for droplet inertia. Introducing $\tau_{*n} = V_g(r_n)/g$ and using (88) makes it possible to rewrite the MB model as

$$K_{n\mathrm{MB}} = \frac{\nu_t}{Sc_T}\left[1+\frac{1.56 u_*^2\, V_g(r_n)}{g\, \nu_t(z)}\right]^{-1} \tag{91}$$

It is interesting to see that the three models result in three relationships (83), (89) and (91) that have functional resemblances, but different dependencies on V_g and u_*.

Figures 16 to 19 compare the concentration profiles, normalized by the surface flux, obtained with SeaCluse in nonevaporative conditions with these three models of turbulent diffusivity, for each of the four typical categories 10-, 60-, 100-, 250-μm radius, and for the two wind speeds, 20 and 10 m/s. The wave parameters are h = 0.135 and Γ = 0.85. Each figure includes two frames, with (a) the three turbulent profiles on a log-linear plot covering the whole domain of calculation at 20 m/s, and (b) the profile obtained with the MB model in a Cartesian plot that also contains the nonturbulent profiles $\xi_n(z)$ computed by the preprocessor (dots), in the lower part of the domain and especially between wave trough and crest (see the height scale normalized by H_o on the right side of the frames). In addition the frames (a) show for comparison the profiles obtained at 10 m/s with the MB model (plotted versus z, not versus z/H_o). The calculation grid is designed with great care to satisfy the numerical solver requirements [see *Rouault et al.*, 1991; *Schiestel*, 1993; *Van Eijk et al.*, 1993]. The required spacing appears to be of the order of the value of the eddy diffusivity. A logarithmic grid [*Rouault et al.*, 1991] of 50 grid points is introduced in the wave trough region, with meshes ranging from 10^{-5} m to about 1–5 cm. The remainder of the wave region is covered by a constant mesh grid, and the upper region by a logarithmic grid extending from the

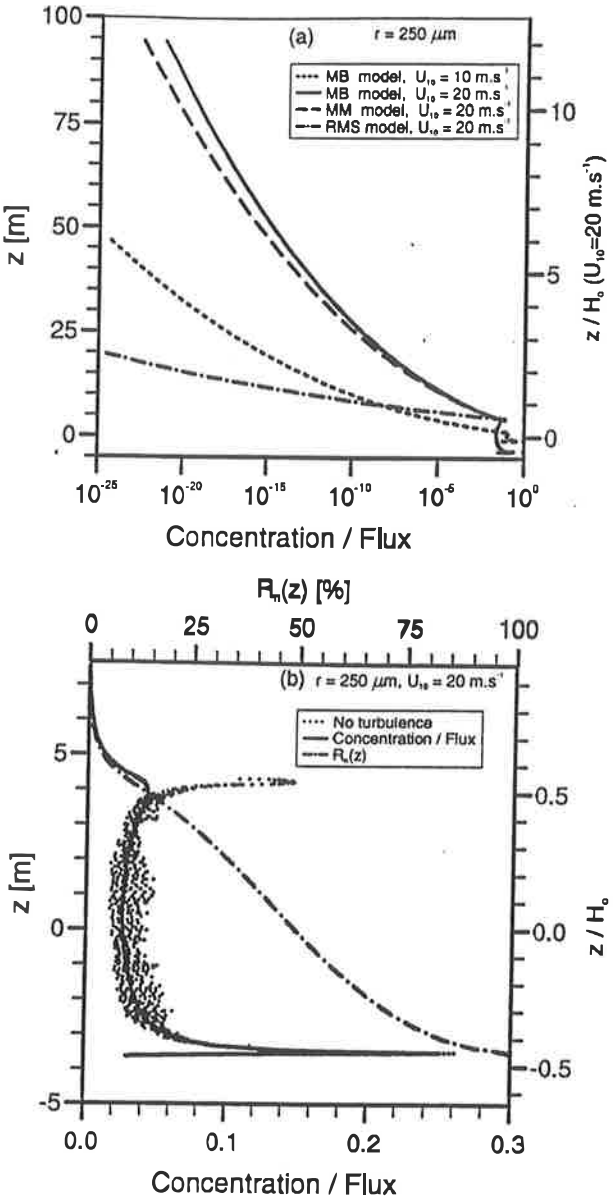

Figure 16. Profiles of concentration normalized by the surface flux for droplets of 250-μm radius (a) in the entire domain of calculation, with the three models of turbulence at 20 m/s and with the MB model at 10 m/s, and (b) in the wave region, without turbulence (dots) and with turbulence (MB model). In addition, Figure 16b displays the integral ratio $R_n(z)$.

wave crests ($z = 0.53 H_o$) to the top of the calculation domain ($z = z_{max}$) where the grid spacing is typically 1–5 m. The total number of grid points is of the order of 200–500. Here, with z_{max} = 100 m, the numbers of calculation points are 50, 252, and 210, in each of the three domains respectively, summing to 512, for all droplet categories. Figures 16–19 call for several comments. The first general comment is that the three largest droplet categories manifest somewhat similar behavior, with size-dependent details, while the 10-μm category behaves somewhat differently because of its reduced weight and inertia. This is why the display ranges are different in Figures 16-18 from that of Figure 19. The two types of behavior are discussed separately. Note that on the right side of the frames the altitude z is normalized with the value of H_o at U_{10} = 20 m/s.

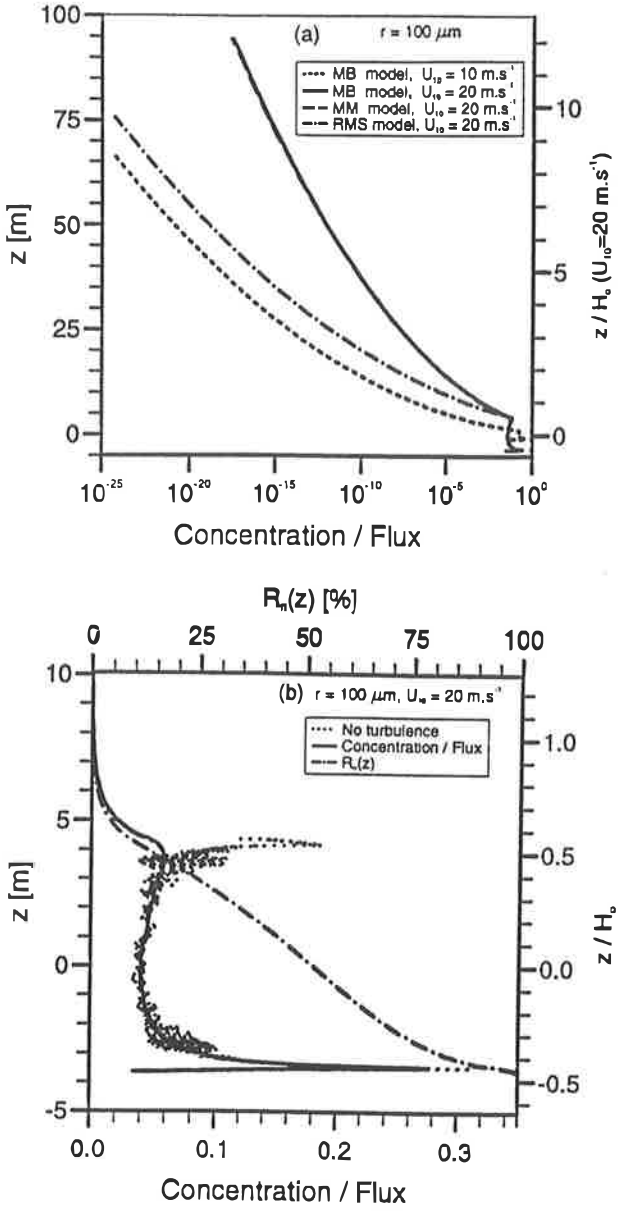

Figure 17. Same as Figure 16, but for $r = 100$ μm.

Consideration of the nonturbulent profiles (dots in frames b) shows that the rotor-like flow structure is a rather efficient transport mechanism for the droplets when compared to the profiles obtained over a flat surface [see *Rouault et al.*, 1991, Figure 5]: 70 to 80% of the droplets are transported higher than $-H_o/4$ and about 25% reach the wave crest height. For the largest droplets, the observation of similar plots at various wind speeds (not shown here) shows that the vertical transport seems relatively less efficient at higher wind speed (i.e., when compared in relative scale z/H_o), but this is largely compensated for by the increase of H_o with U_{10}. For the 10-μm droplets, the transport efficiency is even larger, since more than 80% of the droplets are transported to around the wave crest level or higher. At lower wind speed, although weaker in strength, the rotor-like flow becomes relatively more efficient for the transport of the smaller droplets because it takes place much higher with respect to the wave height: for U_{10} = 10 m/s its center is at $z = H_o$ and it extends up to z = 2-2.5 H_o.

As regards the turbulent diffusivity, the two models MM and MB appear to produce unexpectedly close results, considering their functional differences: it is only for the largest droplets (250 μm) that they introduce noticeable differences in the higher part of the concentration profiles (although the difference increases at lower wind speeds); note, however, the considerable range of concentrations in the logarithmic scale of frames a. Compared to these two models, *Rouault et al.*'s [1991] diffusivity reduction due to inertia appears to increase much more rapidly with increasing droplet size, reducing the diffusion of the 250-μm droplets by turbulence to practically zero. For the 10-μm droplets, the effect of inertia is so small that the lines corresponding to the three different models cannot be separated.

The primary effect of turbulent diffusion, mixing, is to reduce the gradients and to smooth the peaks. This is clearly illustrated in the b' frames, where the low-level profiles are well smoothed, although the very weak diffusivity in the wave trough is unable to erase the lowest peaks. Since the concentrations are zero at the top of the calculation domain, the secondary effect of turbulent diffusion is to transfer droplets upward, from high concentration layers to low concentration layers. The efficiency of the transport by turbulence is demonstrated by the additional curves of frames

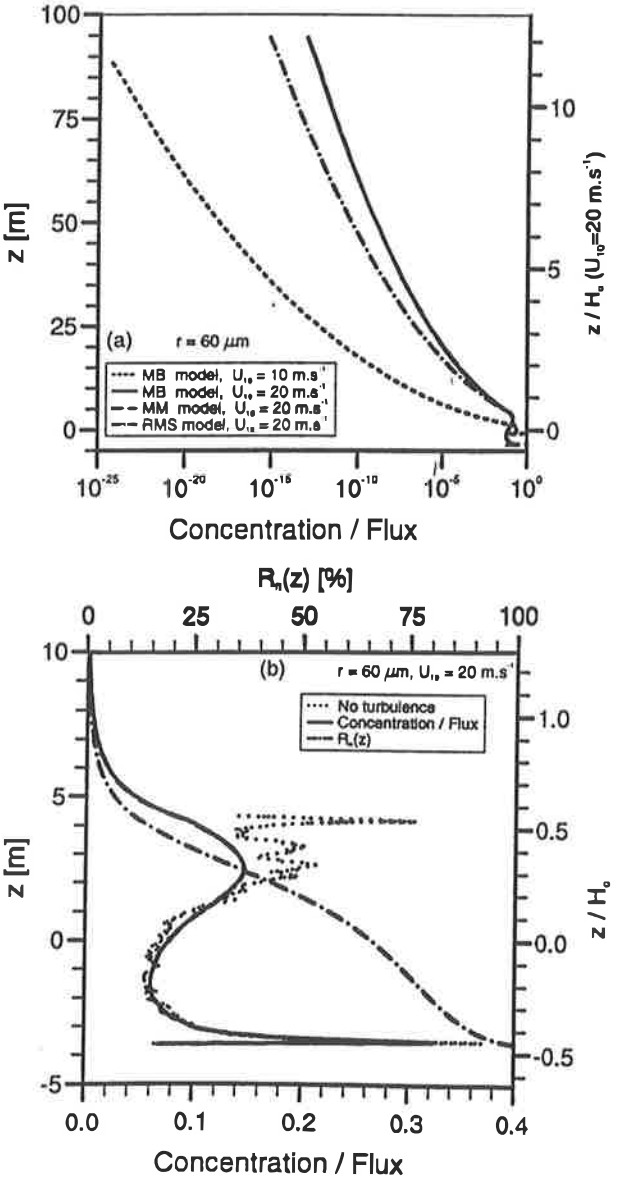

Figure 18. Same as Figure 16, but for $r = 60$ μm.

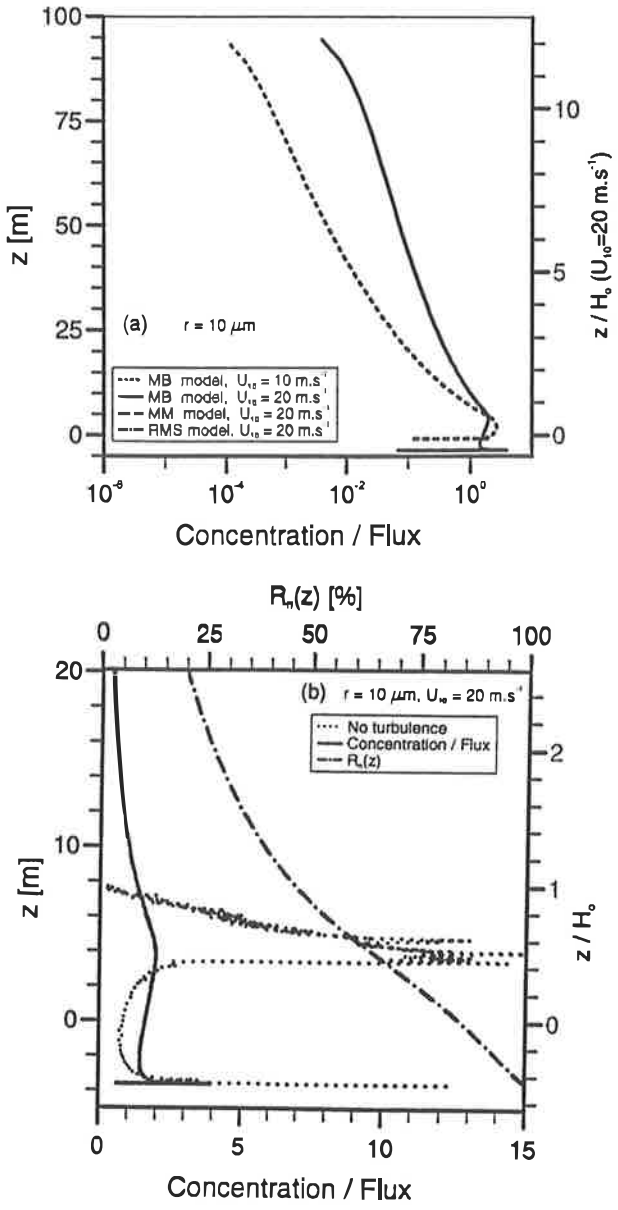

Figure 19. Same as Figure 16, but for $r = 10\ \mu m$.

b obtained by computing the integrals

$$R_n(z) = \int_z^{z_{max}} \rho_n(z')\, dz' \Big/ \int_{z_{min}}^{z_{max}} \rho_n(z')\, dz' \qquad (92)$$

from the results of the simulations with the MB model at 20 m/s. $R_n(z)$ indicates how much of the droplet population has been transported higher than z. For instance, it appears that only about 10% of the droplets are transported by turbulence higher than the highest level reached without turbulence, except for the 10-μm droplets that are well transported upward and for which this number is of the order of 50%. For those droplets that have non-negligible inertia and weight, turbulence does not appear to be a very efficient transport process. Except for the smallest category, no more than 12-18% of the droplets reach the wave crest level or go higher, and no more than 3–5% at 20 m/s (1–2% at 10 m/s) reach a level 1 m above the wave crest. This last comment addresses the experimental attempts to deduce the surface source function from the droplet concentrations measured in the atmosphere, i.e., with the above-down method. Figures 16-19 show that the concentrations decrease very rapidly with increasing height, e.g., they are about 2 orders of magnitude smaller at 10 m than at wave crest level, and they do not exhibit constant-slope ranges in the log-linear plots that would correspond to exponential laws. This demonstrates that the above-down method to deduce the surface flux function from fits to experimental data can easily produce erroneous estimates. The errors can be extremely large if the number of measurement levels is small and the model used to analyze the data is too crude or poorly assessed, especially since droplet partial evaporation is expected to highly complicate the transfer functions.

Finally, it can be noted from a consideration of the upper end of the profiles in frames a that the boundary condition of zero droplet concentration is well obeyed by all droplet categories except the smallest one, which obviously reflects a thwarted tendency to diffuse higher than 100 m.

5. Conclusions

The preceeding sections have presented the first steps in the construction of a numerical code having capabilities to simulate most of the dynamics of the evaporating sea spray droplets, their behavior, and their influence on the structure of the lower marine atmosphere. It should, in principle, be able to describe and quantify the nonlinear interactions between the droplets and the scalar fields of water vapor concentration and temperature. It would be useful in the assessment of the spray surface source function. Finally, it will be able to predict the marine aerosol content of the atmospheric surface layer as a function of the basic micrometeorological parameters.

The code includes two parts: the preprocessor computes the air flow structure and the droplet trajectories over the waves in the absence of turbulence and evaporation, while the main program computes along the vertical the local budgets of droplet and water vapor concentrations, and sensible heat, including the dynamic and thermodynamic air-droplet interactions. To minimize the model artifacts, it is constructed on a small number of robust assumptions, as e.g., the horizontal homogeneity of the momentum transfer from the air to the sea surface. Also, to keep the model simple during the period of its construction and validation, several restrictive assumptions are provisionally introduced in the mean air flow description:

1. The wave field is modeled by a 2-D Stokes wave.
2. The waves are fully developed and they travel in the direction of the wind.
3. Momentum is only transferred to the water surface, with no form drag.

An additional hypothesis is introduced to describe the motion of the droplets in the mean air flow: the droplet flight times in nonturbulent and nonevaporative conditions are finite. Also, the evaporation model of *Mestayer* [1990] includes assumptions that restrict its validity domain [*Van Eijk et al.* 1993]. However, the code is constructed with a deep modular structure, allowing easy introduction of advanced or additional models. For instance, the above assumptions on the wave field, that limit the model use to open ocean, will be relaxed with the introduction of a wave field model for coastal areas, currently in development [*Mestayer*, 1991], while a more realistic description of the air flow over breaking waves probably requires an asymmetric wave model. Also, while the model for spume droplet initial dynamics is still in construction, the source function module is constructed as a "tool-box" for introducing the corresponding additional sources. The results presented here make it possible to surmise that the

largest droplet concentrations exist on the lee side of the waves, based on the extended droplet suspension times at that location and the observation of droplet trajectories. This is in agreement with laboratory experiments by *Koga and Toba* [1981], who also observed larger concentrations on the lee side of the waves, resulting from droplets produced on the downward slope of the same wave trough. On the other hand, *De Leeuw* [1989a] indicated that in the field the production may be higher on the windward side of the crest because the whitecap of a trailing wave can be at the windward side of the crest. These observations form some of the bases for the construction of the advanced droplet source module.

To avoid entering prematurely into a controversial choice of the empirical droplet surface source function, in the first simulations presented here the droplet concentrations are normalized by their surface flux. These simulations provide several results on the dynamics of the droplets over the waves (without evaporation). The mean air flow induced by the motion of the wavy surface results into a large rotor-like structure whose position and intensity depend on the wind speed and wave amplitude. This mean flow appears as a powerful transport process for the droplets of all sizes, typically propelling a large proportion of them about the wave crest height $H_o/2$ or even higher. Due to the displacement of the center of the rotor-like structure, the efficiency of this transport process decreases relatively with increasing wind speed. This relative decrease is more than compensated for by the increase in wave height, which is proportional to the square of the wind speed. Yet, this transport does not appear to change dramatically the trajectories of most droplets. Although those that are ejected from the lee side of the waves see their trajectories greatly lengthened, the smallest of them even entering in closed-loop or very long spiralling trajectories, on average, the final fall velocities and the flight times of the droplets larger than about 90 μm do not differ much from those observed over a flat surface, while the smallest droplets have greatly lengthened flight times. The average flight times, as well as the maximum flight times, of the medium and large droplets appear to depend rather weakly on the wind speed and to increase much less rapidly than the wave height, in contradiction with the model of residence times equal to $H_{1/3}/V_g$, increasing as U_{10}^2.

Andreas [1992] proposed this model for the droplet residence time in the presence of turbulence, while the results of Figures 13-15 are obtained without turbulent diffusion, reflecting essentially the influence of the droplet transport by the wave-induced movement. Can this account for the difference in the wind dependence of T_{fly} ? It must first be noted that *Andreas'* [1992] formula, $T_{fly} = H_{1/3}/V_g$, obviously reflects the influence of the wave-induced movement more than that of turbulence, since it parameterizes the mean residence time as a that of a simple gravitational fall from the height of the significant wave but does not include any parameterization of the turbulent diffusivity. Second, the results of Figures 16-19 illustrate well that the role of turbulence is much more to diffuse than to transport. Diffusion by turbulence does smooth concentration profiles and tends to rub out their peaks. For the passive scalars, the gases, and the small droplets that have a negligible weight, this diffusion does generate an important transfer from the regions where the concentrations are high toward those where the concentrations are low; but for those larger droplets that have nonnegligible weights, the downward gravitational flux opposes the turbulent transfer, while this transfer is also reduced because these droplets have nonnegligible inertia. Figures 16-19 show that only a very small part travel higher over the waves in the presence of turbulent diffusion than without turbulence. Third, since the wave-induced movement is accounted for in the mean movement, the influence of turbulent diffusion can be parameterized with the turbulence timescale, which is proportional to the eddy viscosity ν_t, i.e., $\sim U_{10}$ (see (43)-(46) and (88).) In conclusion, we think that, although turbulence does increase the flight times of the small percentages of droplets which are entrained in the upper layers, it does not increase largely the average flight times of most droplet categories (typically, $r > 60$ μm). Our results show that modeling the residence time with $H_{1/3}/V_g$ most certainly overestimates them largely at high wind speeds. This conclusion can be of great importance for the development of simplified models such as box models, or two-layer models, where the influence of turbulence on the residence times and droplet transport are prescribed.

Turbulence appears here to have a weak influence on the vertical profiles of most droplet concentrations: these profiles are mainly determined by the structure of the mean flow induced by the wave motion, and only extremely small concentrations are diffused higher than the wave region. Should it be concluded that the precision of the turbulence model for droplets, i.e., the inertial reduction of turbulent diffusivity, is of little importance compared to that of the model of the air flow over the waves ?

In answering this question, several points must be considered.

1. While the model of the wave field is obviously of crucial importance since a large amount of droplets are concentrated around the level of the wave crest, it is not obvious that the detailed structure of the mean flow is of comparable importance, due to the horizontal averaging process to obtain $\xi(z)$ and $\rho_n^o(z)$; this is the subject of current systematic studies.

2. To estimate the contribution of spray droplets to the humidity flux from a known surface source function, the turbulence model is possibly of relatively small influence, since the droplets that contribute most to the humidity flux are not greatly displaced by diffusion and therefore evaporate in a relatively thin layer around the wave crest level.

3. The previous point is true only if the humidity and temperature profiles do not exhibit very large gradients in this layer, and if the wind speed is not extreme. In conditions of very strong winds, which are the most important in this issue, the wave crests are very high, the turbulent diffusion is very strong, and the droplet turbulence models diverge for relatively small droplet sizes, in the range of the most productive droplets. Moreover, the precise quantitative assessment of the nonlinear negative feedback in the humidity flux requires a precise description of the droplet dynamics in this evaporation layer.

4. The droplet diffusion model is obviously of the greatest importance when the desired outputs are the vertical profiles of droplet concentrations and the atmospheric aerosol content close to, and away from, the sea surface (e.g., to compute the effects of aerosols on the electrooptical properties of the atmosphere).

5. Finally the diffusion model is of crucial importance for determining the surface source function from the above-down method, or to validate it, because in the open ocean, experimental data are rarely obtained with precision at levels lower than deck height, and are often obtained at markedly higher elevations with airborne sensors.

Since the present simulations showed a relatively good convergence of the MM and MB models derived from *Mostafa and Mongia* [1987] and *Melville and Bray* [1979] and a rather large divergence from the RMS model of *Rouault et al.* [1991] it seems necessary to proceed to an independent reassessment. This

is one of the studies in progress, which also include a series of tests and validations versus experimental data from the HEXOS program [*De Leeuw*, 1990].

This paper does not present direct comparisons of the simulations with open sea measurements because no surface source function has been selected yet. In addition, these simulations use a homogeneous distribution of the surface sources, as expected for the bubble-generated jet drops. To simulate spume drops, not only a quantitative spectral source function is required, but also the spatial distribution of their sources and their initial velocity, which implies a much better knowledge of their generation process and initial kinematics than is available in the literature. Observational efforts are needed. Finally, it must be stressed again that, up to now, the basic assumptions of the mean flow preprocessor are consistent with high but not extreme wind conditions and fully developed wave fields. For other conditions, including coastal seas and sea states with a large number of steep and breaking waves, these assumptions will need to be revised. The preprocessor can also be improved by taking into account not only the shape of the average wave, but that of several waves.

Theoretically, the smallest droplets that can be handled by the SeaCluse model have a radius of 1 μm. However, computational demands become rather high when the droplet radius is of the order of a few microns. This is a severe drawback for the application of the model in range prediction, since droplets with radii smaller than 10 μm determine the visibility in the visible wavelength region and contribute appreciably to the visibility in the IR. In order to overcome this drawback, the CLUSA model is being developed to describe the dispersion of a distribution of aerosols from 0.05- to 2.5-μm radius in the marine atmospheric surface layer with an emphasis on the dry deposition process and the effect of Brownian diffusion [*Mestayer et al.*, 1991]. It is expected in the future to merge the two models or to introduce the small droplets in SeaCluse, using more realistic boundary conditions at the top of the domain. The code could then include some interactions of the smaller aerosols with sea spray droplets by coalescence.

Presently, the SeaCluse code only deals with freshly produced seaspray aerosols. The total aerosol concentration in the atmosphere results from a balance between local production and removal and the advection of aerosol produced elsewhere. It is conjectured that the advected aerosol is in effect a "background" that adds to the profile due to locally produced aerosol. In view of the long mixing times of the former, the latter constitutes only a small fraction of the total aerosol concentration. The background aerosol consists of a mixture of man-made, biological, and natural aerosol of continental and marine origin, containing a large variety of hygroscopic and nonhygroscopic species which strongly influence the dependence on relative humidity. Furthermore, aerosol droplets are not inert, and their composition can change through many chemical reactions which take place in the atmosphere. *Van Eijk and De Leeuw* [1992] recently addressed the importance of taking the background aerosol of continental origin into account when predicting propagation parameters (e.g., atmospheric extinction) for a coastal region. Apparently, well-established aerosol models such as the Navy Aerosol Model [*Gathman*, 1983] fail for "polluted inner seas" like the North Sea and the Mediterranean Sea [*Tanguy et al.*, 1991]. In conclusion, a model that aims to provide an adequate description of the propagation properties of the atmosphere cannot be confined to the freshly produced sea-salt aerosols. In addition, modules that handle the continuously changing chemical composition and the dispersion of the "background" aerosols are needed. Only then can the resulting aggregate model truly describe the production, advection, and deposition of the aerosols.

Acknowledgments. This work has been sponsored in part by the Commission of the European Communities (EC DG XII contracts STEP-CT-0047 and EV5V-CT93-0313), by the U.S. Office of Naval Research (N00014-94-1-0498), by the Netherlands Ministry of Defence (A90KM638), and as an EUROTRAC Air-Sea Exchange Contribution, by the French Centre National de la Recherche Scientifique (92N82/0019 Environnement). Part of the work described in this report was performed while A.M.J. Van Eijk held the position of Enseignant Invité at the Ecole Centrale de Nantes. Special thanks are due to the three reviewers of this manuscript for many comments and suggestions. HEXOS contribution 43.

References

Andreas, E.L., Thermal and size evolution of sea spray droplets, *CREEL-Report 89-11*, Cold Reg. Res. and Engi. Lab., Hanover, N.H., USA, 1989.

Andreas, E.L., Time constants for the evolution of sea spray droplets, *Tellus, 24B*, 481-497, 1990a.

Andreas, E.L., Model estimates of the effects of sea spray on air-sea heat fluxes, in *Modeling the Fate and Influence of Marine Spray, Whitecap Rep. 7*, edited by P.G. Mestayer, E.C. Monahan, and P.A. Beetham, pp. 115-127, Mar. Sci. Institute, University of Connecticut, 1990b.

Andreas, E.L., Sea spray and turbulent air-sea fluxes, *J. Geophys. Res., 97*, 11,429-11,441, 1992.

Andreas, E.L., Reply, *J. Geophys. Res., 99*, 14,345-14,350, 1994.

Andreas, E.L., J.B. Edson, E.C. Monahan, M.P. Rouault, and S.D. Smith, The spray contribution to net evaporation from the sea: A review of recent progress, *Boundary Layer Meteorol., 72*, 3-52, 1995.

Baldy, S., Bubbles in the close vicinity of breaking waves: Statistical characteristics of the generation and dispersion mechanism, *J. Geophys. Res., 93*, 8239-8248, 1988.

Beard, K.V., and H.R. Pruppacher, A wind tunnel investigation of the rate of evaporation of small water droplets falling at terminal velocity in air, *J. Atmos. Sci., 28*, 1455-1464, 1971.

Blanchard, D.C., The electrification of the atmosphere by particles from bubbles in the sea, *Prog. Oceanogr., 1*, 71-202, 1963.

Blanchard, D.C., The production, distribution, and bacterial enrichment of the sea-salt aerosol, in *Air-Sea Exchange of Gases and Particles*, edited by P.S. Liss and W.G.N. Slinn, pp. 407-454, D. Reidel, Norwell, Mass., 1983.

Blanchard, D.C., The size and height to which jet droplets are ejected from bursting bubbles in seawater, *J. Geophys. Res., 94*, 10,999-11,002, 1989.

Blanchard, D.C. and A.H. Woodcock, The production, concentration and vertical distribution of the sea-salt aerosol, *Ann. NY Acad. Sci., 338*, 330-347, 1980.

Buck, A.L., New equation for computing vapor pressure and enhancement factor, *J. Appli. Meteorol., 20*, 1527-1532, 1981.

Charnock, H., Wind stress on a water surface, *Q. J. R. Meteorol. Soc., 81*, 639-640, 1955.

DeCosmo, J., K.B. Katsaros, S.D. Smith, R.J. Anderson, W.A. Oost, K. Bumke, and H. Chadwick, Air-sea exchange of water vapor and sensible heat: The Humidity Exchange over the Sea (HEXOS) results. *J. Geophys. Res., 101*, 12,001- 12,016, 1996.

Dekker, H., and G. De Leeuw, Bubble excitation of surface waves and aerosol droplet production: a simple dynamical model, *J. Geophys. Res., 98*, 10,223-10,232, 1993.

De Leeuw, G., Vertical profiles of giant particles close above the sea surface, *Tellus, 38B*, 51-61, 1986.

De Leeuw, G., Near-surface particle size distributions profiles over the North Sea, *J. Geophys. Res., 92,* 14,631-14,635, 1987.

De Leeuw, G., Survey of the CLUSE main experiment Grand-CLUSE, *TNO rep. FEL 1988-43,* TNO (Netherlands organization for applied scientific research), the Netherlands, 1988.

De Leeuw, G., Investigations on turbulent fluctuations of particle concentrations and relative humidity in the marine atmospheric surface layer, *J. Geophys. Res., 94,* 3261-3269, 1989a.

De Leeuw, G., The occurrence of large salt water droplets at low elevations over the open ocean, in *The Climate and Health Implications of Bubble Mediated Sea-Air Exchange, Conn. Sea Grant Coll. Prog. CT-SG-89-06,* edited by E.C. Monahan and M.A. Van Patten, pp. 65-82, Groton, Conn., 1989b.

De Leeuw, G., Profiling of aerosol concentrations, particle size distributions and relative humidity in the atmospheric surface layer over the North Sea, *Tellus, 42B,* 342-354, 1990a.

De Leeuw, G., Comment on "Vertical distributions of spray droplets near the sea surface: Influences of jet drop ejection and surface tearing," by J.Wu, *J. Geophys. Res., 95,* 9779-9782, 1990b.

De Leeuw, G., Aerosols near the air-sea interface, *Trends Geophys. Res., 2,* 55-70, 1993.

De Leeuw, G., K.L. Davidson, S.G. Gathman, and R.V. Noonkester, Physical models for aerosols in the marine mixed layer, *AGARD Conf Proc. 453,* 40-1 to 40-8, 1989.

Donelan, M.A., and W.H. Hui, Mechanics of ocean surface waves, *Surface Waves and Fluxes, vol. I,* edited by G.L. Geernaert and W.J. Plant, pp. 209-246, Kluwer Acad Press, Norwell, Mass., 1990.

Edson, J.B., Lagrangian model simulation of the turbulent transport of evaporating jet droplets, Ph.D. thesis, Dep. of Meteorol., Penn. State Univ., University Park, 1989.

Edson, J.B., Simulating droplet motion above a moving surface, in *Modeling the Fate and Influence of Marine Spray, Whitecap Rep. 7,* edited by P.G. Mestayer, E.C. Monahan, and P.A. Beetham, pp. 84-94, Mar. Sci. Institute, University of Connecticut, 1990.

Edson, J.B., and C.W. Fairall, Spray droplet modeling I: Lagrangian model simulation of the turbulent transport of evaporating spray droplets, *J. Geophys. Res., 99,* 25,295-25,311, 1994.

Edson, J.B., C.W. Fairall, P.G. Mestayer, and S.E. Larsen, A study of the inertial dissipation method for computing air-sea fluxes, *J. Geophys. Res., 96,* 10,689-10,711, 1991.

Edson, J.B., S. Anquetin, P.G. Mestayer, and J.F. Sini, Spray droplet modeling II: An interactive Eulerian-Lagrangian model of evaporating spray droplets, *J. Geophys. Res., 101,* 1279-1299, 1996.

Fairall, C.W., Modeling the fate and Influence of marine spray: a review, in *Modeling the Fate and Influence of Marine Spray, Whitecap Rep. 7,* edited by P.G. Mestayer, E.C. Monahan, and P.A. Beetham, pp. 1-16, Mar. Sci. Institute, University of Connecticut, 1990.

Fairall, C.W., and J.B. Edson, Modeling the droplet contribution to the sea-to air moisture flux, in *The Climate and Health Implications of Bubble Mediated Sea-Air Exchange, Conn. Sea Grant Coll. Prog. CT-SG-89-06,* edited by E.C. Monahan and M.A. Van Patten, pp. 121-146, Groton, Conn., 1989.

Fairall, C.W., K.L. Davidson, and G.E. Schacher, An analysis of the surface production of sea-salt aerosols, *Tellus, 35,* 31-39, 1983.

Fairall, C.W., J.D. Kepert, and G.J. Holland, The effect of sea spray on surface energy transports over the ocean, *Global Atmos. Ocean Syst., 2,* 121-142, 1994.

Gathman, S.G., Optical properties of the marine aerosol as predicted by the Navy Aerosol Model, *Opt. Eng., 22,* 57-62, 1983.

Gathman, S.G., A preliminary description of NOVAM, the Navy Oceanic Vertical Aerosol Model, *NRL Rep. 9200,* Nav. Res. Lab., Washington, D.C., 1989.

Geernaert, G.L., Drag coefficient modeling for the coastal zone, *Dyn. Atmos. Oceans, 11,* 307-322, 1988.

Geernaert, G.L., Bulk parameterizations for the wind stress and heat fluxes, in *Surface Waves and Fluxes,* vol. I, edited by G.L. Geernaert and W.J. Plant, pp. 91-172, Kluwer Acad., Norwell, Mass., 1990.

Geernaert, G.L., K.B. Katsaros, and K. Richter, Variation of the drag coefficient on sea state, *J. Geophys. Res., 91,* 7667-7679, 1986.

Gerber, H.E., Relative humidity parameterization of the Navy Aerosol Model (NAM), *NRL Rep. 8956,* Nav. Res. Lab., Washington, D.C., 1985.

Högström, U., Non-dimensional wind and temperature profiles in the atmospheric surface layer: A re-evaluation, *Boundary Layer Meteorol., 42,* 55-78, 1988

Hughes, H.G. Evaluation of the LOWTRAN 6 Navy maritime aerosol model using 8 to 12 μm sky radiances, *Opt. Eng., 26,* 1155-1160, 1987.

Janssen, P.A.E.M., P. Lionello, and L. Zambretsky, On the interaction of wind and waves, *Philos. Trans. R. Soc. London A, 329,* 289-301, 1989.

Katsaros, K.B., and G. De Leeuw, Comment on "Sea spray and the turbulent air-sea heat fluxes" by E.L. Andreas, *J. Geophys. Res., 99,* 14,339-14,343, 1994.

Kitaigorodskii, S.A., O.A. Kuznetsov, and G.N. Panin, Coefficients of drag, sensible heat, and evaporation in the atmosphere over the surface of the sea, *Izv. Atmos. Ocean. Phys., 9,* 1135-1141, 1973.

Kneizys, F.X., E.P. Shettle, W.O. Gallery, J.H. Chetwynd Jr., J.H. Abreu, J.E.A. Selby, S.A. Clough, and R.W. Fenn, Atmospheric transmittance/radiance: Computer code LOWTRAN 6, *Rep. AFGL-TR-83-0187,* Air Force Geophys. Lab., Hansom Air Force Base, Bedford, Mass., 1983.

Koga, M., and Y. Toba, Droplet distributions and dispersion processes on breaking wind waves, *Sci. Rep. Tohoku Univ. Ser. 5, 28,* 1-25, 1981.

Ling, S.C., and T.W. Kao, Parameterization of the moisture and heat transfer process over the ocean under whitecap sea states, *J. Phys. Oceanogr., 6,* 306-315, 1976.

Ling, S.C., T.W. Kao, and A.I. Saad, Microdroplets and transport of moisture from the ocean, *Proc. Am. Soc. Civ. Eng. Mech. Div., 106,* 1327-1339, 1980.

Maat, N., C. Kraan, and W.A. Oost, The roughness of wind waves, *Boundary Layer Meteorol., 54,* 89-103, 1991.

MacIntyre, F., A boundary layer "microtome" for micron thick samples of a liquid surface, *J. Phys. Chem., 72,* 589, 1968.

MacIntyre, F., Flow patterns in breaking bubbles, *J. Geophys. Res., 77,* 5211-5228, 1972.

Meek, C.C., and B.G. Jones, Studies of the behavior of heavy particles in a turbulent fluid flow, *J. Atmos. Sci., 30,* 239-244, 1973.

Melville, W.K., and K.N.C. Bray, A model of the two-phase turbulent jet, *Int. J. Heat Mass Transfer, 22,* 647-656, 1979.

Mestayer, P.G., Sea water droplet evaporation in the CLUSE

model, in *Modeling the Fate and Influence of Marine Spray, Whitecap Rep. 7*, edited by P.G. Mestayer, E.C. Monahan, and P.A. Beetham, pp. 65-76, Mar. Sci. Institute, University of Connecticut, 1990

Mestayer, P.G., Modèle synthétique de profils de vent et de diffusivité turbulente au dessus de la surface marine côtière, *Note interne LMTTD-H.91.01*, Ecole Centrale de Nantes, France, April 1991.

Mestayer, P.G., and C. Lefauconnier, Spray droplet generation, transport and evaporation in tunnel during the Humidity Exchange Over the Sea Experiments in simulation tunnel, *J. Geophys. Res., 93*, 572-586, 1988.

Mestayer, P.G., J.B. Edson, C.W. Fairall, S.E. Larsen, and D.E. Spiel, Turbulent transport and evaporation of droplets generated at an air-water interface, in *Turbulent Shear Flows 6*, edited by J.C. André et al., pp. 129-147, Springer-Verlag, New York, 1989.

Mestayer, P.G., E.C. Monahan and P.A. Beetham, (Eds.) *Modeling the Fate and Influence of Marine Spray, Whitecap Rep. 7*, Mar. Sci. Institute, University of Connecticut, 1990.

Mestayer, P.G., J.B. Edson, M.P. Rouault, C.W. Fairall, S.E. Larsen, G. De Leeuw, D.E. Spiel, J. DeCosmo, K.B. Katsaros, E.C. Monahan, and R. Schiestel, CLUSE simulations of the vapor flux modification by droplet evaporation, in *Modeling the Fate and Influence of Marine Spray, Whitecap Rep. 7*, edited by P.G. Mestayer, E.C. Monahan, and P.A. Beetham, pp. 100-105, Mar. Sci. Institute, University of Connecticut, 1990.

Mestayer, P.G., A. Zoubiri, and J.B. Edson, Experimental and numerical study of aerosol dynamics and deposition at the sea surface; 2PIE, GWAIHIR & CLUSA, *EUROTRAC Ann. Rep. 1990*, pp. 66-74, Fraunhofer Inst., Garmisch-Partenkirchen, Germany, 1991.

Miller, M.A., An investigation of aerosol generation in the marine planetary boundary layer, M.S. thesis, Dep. of Meteorol., Penn. State Univ., University Park, 1987.

Miller, M.A., and C.W. Fairall, A new parameterization of spray droplet production by oceanic whitecaps, in *Proceedings of the 7th Conference on Ocean-Atmosphere Interaction, Feb. 1-5, Anaheim, CA*, pp. 174-177, Am. Meteorol. Soc., Boston Mass., 1988.

Monahan, E.C., K.L. Davidson, and D.E. Spiel, Whitecap aerosol productivity deduced from simulation tank measurements, *J. Geophys. Res., 87*, 8898-8904, 1982.

Monahan, E.C., D.E. Spiel, and K.L. Davidson, A model of marine aerosol generation via whitecaps and wave disruption, in *Oceanic Whitecaps*, edited by E.C. Monahan and G. McNiocaill, pp. 167-174, D. Reidel, Norwell, Mass., 1986.

Monin, A.S. and A.M. Yaglom, *Statistical Fluid Mechanics: Mechanics of Turbulence*, MIT Press, Cambridge, Mass., 1987.

Mostafa, A.A., and S.E. Elgobashi, A study of the motion of vaporizing droplets in a turbulent flow, in *Dynamics of Flames and Reactive Systems*, edited by J.R. Bowen et al., *Progr. Astronaut. Aeronaut., 95*, 513, 1984.

Mostafa, A.A., and H.C. Mongia, On the modeling of turbulent evaporating sprays: Eulerian versus Lagrangian approach, *J. Heat Mass Transfer, 12*, 2583-2593, 1987.

Panofsky, H.A. and J.A. Dutton, *Atmospheric Turbulence*, John Wiley, New York, 1984.

Pruppacher, H.R. and J.D. Klett, *Microphysics of Clouds and Precipitation*, D. Reidel, Norwell, Mass., 1978.

Raudviki, A.J., *Loose Boundary Hydraulics*, Pergamon, New York, 1979.

Rouault, M.P., Modélisation numérique d'une couche limite unidimensionelle stationnaire d'embruns, Thèse de Doctorat, Univ. d'Aix-Marseille II, France, 1989.

Rouault, M.P. and S.E. Larsen, Spray droplets under turbulent conditions, *Rep. Risø-M-2847*, Risø Natl. Lab., Denmark, 1990.

Rouault, M.P., P.G. Mestayer, and R. Schiestel, A model of evaporating spray droplet dispersion, *J. Geophys. Res., 96*, 7181-7200, 1991.

Schiestel, R., *Modélisation et Simulation Numérique des Écoulements Turbulents*, Editions Hermes, Paris, France, 1993.

Slinn, S:A., and W.G.N. Slinn, Modeling of atmospheric particulate deposition to natural waters, in *Atmospheric Pollutants in Natural Waters*, edited by S.J. Eisenreich, pp. 23-53, Butterworth-Heinemann, Stoneham, Mass., 1981.

Smith, M.H., P.M. Park, and I.E. Consterdine, Marine aerosol concentrations and estimated fluxes over the sea, *Q. J. R. Meteorol. Soc., 119*, 809-824, 1993.

Smith, S.D., Wind stress and heat flux over the ocean in gale force winds, *J. Phys. Oceanogr., 10*, 709-726, 1980.

Smith, S.D., Coefficients for sea surface wind stress, heat flux, and wind profiles as a function of wind speed and temperature, *J. Geophys. Res., 93*, 15467-15472, 1988.

Smith, S.D., Influence of droplet evaporation on HEXOS humidity and temperature profiles, in *Modeling the Fate and Influence of Marine Spray, Whitecap Rep. 7*, edited by P.G. Mestayer, E.C. Monahan, and P.A. Beetham, pp. 171-174, Mar. Sci. Institute, University of Connecticut, 1990.

Smith, S.D., K.B. Katsaros, W.A. Oost, and P.G. Mestayer, Two major experiments in the Humidity Exchange Over the Sea (HEXOS) program, *Bull. Am. Meteorol. Soc., 71*, 161-172, 1990.

Spiel, D.E., Acoustical measurements of air bubbles bursting at a water surface: Bursting bubbles as Helmholtz resonators, *J. Geophys. Res., 97*, 11,443-11,452, 1992.

Spiel, D.E., The sizes of the jet drops produced by air bubbles bursting on sea- and fresh-water surfaces, *Tellus, 46B*, 325-338, 1994.

Stramska, M., Vertical profiles of sea salt aerosol in the atmospheric surface layer: A numerical model, *Acta Geophys. Polonica, 35*, 87-100, 1987

Tanguy, M., H. Bonhommet, M. Autric, and P. Vigliano, Correlation between the aerosol profiles measurements, the meteorological conditions and the IR transmission in a Mediterranean marine atmosphere, *Proc. SPIE Int. Soc. Opt. Eng., 1487*, 17-1 to 17-12, 1991.

Van Eijk, A.M.J and G. De Leeuw, Modeling aerosol extinction in a coastal environment, *Proc. SPIE Int. Soc. Opt. Eng., 1688*, 28-36, 1992.

Van Eijk, A.M.J., P.G. Mestayer, and G. De Leeuw, Conversion of the CLUSE model for applications over open ocean, *TNO Rep. FEL-93-A035*, TNO Defence Res., the Hague, the Netherlands, 1993.

White, F.M., *Fluid Mechanics*, McGraw-Hill, New York, 1988.

Wu, J., Evaporation due to spray, *J. Geophys. Res., 79*, 4107-4109, 1974.

Wu, J., Spray in the atmospheric surface layer: Review and analysis of laboratory and oceanic results, *J. Geophys. Res., 84*, 2959-2969, 1979.

Wu, J., Contributions of film and jet droplets to marine aerosols produced at the sea surface, *Tellus, 41B*, 469-473, 1989.

Wu, J., Vertical distributions of spray droplets near the sea surface: Influences of jet droplet ejection and surface tearing, *J. Geophys. Res., 95*, 9775-9778, 1990.

Wu, J., Production of spume droplets by the wind tearing of wave crests: The search for quantification, *J. Geophys. Res., 98*, 18,221-18,227, 1993.

Wu, J., J.J. Murray, and R.J. Lai, Production and distributions of sea spray, *J. Geophys. Res., 89*, 8163-8169, 1984.

G. De Leeuw and A.M.J. Van Eijk, Physics and Electronics Laboratory TNO, PO Box 96864, 2509 JG Den Haag, the Netherlands (e-mail: deleeuw@fel.tno.nl; amjn1@fel3.fel.tno.nl)

P.G. Mestayer and B. Tranchant, Laboratoire de Mécanique des Fluides, Unité de Recherche Associée au Centre National de la Recherche Scientifique n° 1217, Ecole Centrale de Nantes, 1, rue de la Noë, 44072 Nantes, France (e-mail: patrice.mestayer@ec-nantes.fr; benoit.tranchant@ec-nantes.fr)

(Received January 10, 1995; revised April 23, 1996; accepted April 24, 1996)